Economic Geology, v. 106, pp. 999–1030

Quantifying Metasomatism in Epithermal Au-Ag Deposits: A Case Study from the Waitekauri Area, New Zealand

Mathijs A. Booden,† Jeffrey L. Mauk, and Mark P. Simpson

School of Environment, University of Auckland, Private Bag 92019, Auckland Mail Centre, Auckland 1142, New Zealand

Abstract

Major element geochemical exploration for epithermal deposits can extend the range of traditional pathfinder elements to a 1- to 10-km scale, and with knowledge of protolith composition, mass changes associated with hydrothermal alteration can be quantified. In the Hauraki goldfield of New Zealand, altered andesites and dacites host epithermal Au-Ag deposits and prospects. The major element compositions of equivalent unaltered rocks correlate with whole-rock Zr/TiO_2, an immobile element ratio that is preserved during K metasomatism. We used this feature to estimate the initial composition and calculate a mass balance for veinless altered rocks in the Waitekauri area along a 3-km-wide section that extends from the central Waitekauri fault to the periphery of the alteration zone. The total transferred mass is equal to approximately 11 percent of rock mass in illite-dominated altered rocks, and 24 percent of rock mass in adularia-dominated altered rocks. On average mass losses exceed gains. Potassium was gained in most altered rocks, which contain illite and/or adularia as K-bearing hydrothermal minerals. Silica was gained in adularia-quartz–rich rocks close to the Waitekauri fault. Other major elements are preferentially lost (Ca, Na, Fe, Mg) or effectively immobile (Al, Ti). The greatest K and Si gains occur in adularia-rich rocks that surround Au deposits along the Waitekauri fault, whereas K gains are progressively lower and Si gains are mostly insignificant in deposits and prospects farther east where illite or interstratified illite-smectite is the dominant K-bearing mineral. In contrast, Na and Ca losses do not increase significantly from the periphery to the core of the Waitekauri area, because losses are commonly complete and therefore limited by the initial concentration. However, the K and Si gains correlate with other measures of K metasomatism including K/Sr and Rb/Sr values and molar (*M*) K/(K + Na + 2Ca) values, and together these parameters vector from the barren periphery to the orebody-hosting center of the Waitekauri area. In contrast to major element trends, the pathfinder elements As, Sb, and Hg define more local hydrothermal alteration cells within the larger Waitekauri area, some of which surround Au deposits.

Introduction

Epithermal deposits are surrounded by altered host rocks that have exchanged elements with hydrothermal fluids. The magnitude of gains and losses is generally greatest close to epithermal veins, so a regional gradient in the magnitude of gains and losses can point to epithermal mineralization. Many studies have successfully used trace pathfinder elements, such as As, Sb, Hg, Tl and base metals, for vectoring toward mineralization over distances on the order of tens to hundreds of meters (e.g., White and Hedenquist, 1995; Carlile et al., 1998; Hedenquist et al., 2000). However, because pathfinder elements are mainly confined to veins and adjacent wall rocks, major element mass changes in altered host rocks away from veins have the potential to significantly extend the range of geochemical exploration techniques up to several kilometers (Clarke and Govett, 1990; Madeisky, 1996; Sherlock, 1996; Warren et al., 2007). Nonetheless, major element mass change is difficult to quantify on concentration data alone because major element concentration must sum to 100 percent, which attenuates gains and losses, and compared to pathfinder elements, major element mass changes are small relative to the initial concentration. A mass-balance approach is required to accurately assess major element mass gain and loss, which in turn requires the composition of the protolith to be accurately known. Determining the protolith chemistry of altered rocks has been a hurdle in major element-based exploration techniques, because host rocks typically show incipient to intense alteration in the vicinity of orebodies, which changes their geochemistry, and they also show variable geochemistry away from orebodies; this simply reflects the heterogeneity of all rock units in the Earth's crust but makes it difficult to select a single unaltered host-rock geochemical composition for use in mass-balance calculations (Madeisky, 1996; Sherlock, 1996; Shikazono et al., 2002; John et al., 2003; Leavitt and Arehart, 2005; Gemmell, 2007; Mauk and Simpson, 2007; Warren et al., 2007). MacLean (1990) presented a method to estimate the composition of heterogeneous protoliths to altered rocks on a sample-by-sample basis based on the bulk-rock Zr/TiO_2 ratio, which allows for mass-balance calculations of individual samples without the oversimplifying assumption of a single "representative" unaltered protolith. In this paper we use a variation on MacLean's (1990) approach to assess mass changes in altered volcanic rocks that host gold mineralization in New Zealand.

Epithermal Au-Ag deposits in the Hauraki goldfield, New Zealand, are predominantly hosted in calc-alkaline andesite and dacite of the Coromandel Group. The major element composition of unaltered Coromandel Group rocks correlates with SiO_2 concentration, and the SiO_2 concentration in turn correlates strongly with the ratio Zr/TiO_2. The value of Zr/TiO_2 has been used to characterize protoliths in a range of settings, including altered volcanic rocks in submarine-exhalative (Finlow-Bates and Stumpfl, 1981), altered plutonic rocks in a high-sulfidation Cu-Au deposit (Chambefort et al., 2007), metamorphosed sedimentary rocks (Hickmott and Spear, 1992), and igneous rock type in weathered rocks

† Corresponding author: e-mail, m.booden@auckland.ac.nz

(Hallberg, 1984; Murphy and Stanley, 2007). Zirconium, Ti, and the other high field strength elements (HFSE), which have ionic potential values (ionic charge/radius (Å); Cartledge, 1928) between 3 and 12, are commonly found to be the most immobile elements during open-system alteration in many settings. The HFSE readily hydrolyze in solution and form hydroxides and oxides that are sparingly soluble (Baalen, 1993). Although many studies have found some mobility even of the HFSE during hydrothermal alteration, particularly at very high temperatures or at pH <2.5 (Jiang et al., 2005, and references therein), the HFSE generally represent the best approximation to an immobile element suite. Based on a reference data set of 98 fresh, unaltered Coromandel Group rocks, we establish linear regression equations that relate major element concentrations to Zr/TiO_2. The protolith composition of individual altered Coromandel Group rocks can be estimated based on Zr/TiO_2, because this ratio is relatively unaffected by metasomatic gains and losses of mobile elements. A mass balance can then be calculated for each rock sample. We test our approach on a suite of altered volcanic rocks that have been drilled along a 3-km-wide section, to a depth of several hundred meters; the suite includes rocks that vary from non- to intensely metasomatized. Large sample sets of this type are rare, and the current data provide an outstanding opportunity to critically assess the potential of major element-based whole-rock geochemical exploration.

The Hauraki Goldfield and Hauraki Volcanic Region

The Hauraki volcanic region was the main locus of subduction-related volcanism in northern New Zealand between 18 and 1.95 Ma and records the eruption of basalts, andesites, dacites and rhyolites (Skinner, 1986; Adams et al., 1994; Briggs et al., 2005). The volcanic succession erupted onto Mesozoic Waipapa terrane basement that is exposed in the northern Coromandel peninsula but progressively downfaulted to the south, where the Neogene volcanic succession completely covers the basement rocks. Regional fault sets strike north-northeast and northwest and have similar orientations to epithermal veins (Spörli et al., 2006).

Contained within the Hauraki volcanic region is the Hauraki goldfield, a 100- by 40-km metallogenic province that contains approximately 50 epithermal adularia-sericite Au-Ag deposits and several porphyry Cu-Au-Mo occurrences. Although epithermal deposits occur in andesites, rhyolites, and basement rocks, over 97 percent of gold has been recovered from deposits hosted by altered andesites of the Coromandel Group (Christie et al., 2007). The Coromandel Group erupted between 18 and 2.5 Ma (Stipp, 1968; Adams et al., 1994) and comprises porphyritic basaltic andesites, andesites, and dacites with a phenocryst association of plagioclase ± augite ± hypersthene with minor magnetite, with olivine in some basaltic andesites, and commonly including hornblende (Skinner, 1986). Analogous to modern counterparts in the central North Island (Price et al., 2005), Coromandel Group rocks are mixtures of a relatively silicic (dacitic to rhyolitic) melt, represented by the groundmass, and a gabbroic crystal cargo, which commonly occurs as complexly zoned crystals, angular crystal fragments, and glomerocrysts.

Mining in the Hauraki goldfield between 1852 and 1952 produced over 8 million ounces (Moz) of Au and 35.3 Moz Ag, and an additional 2.1 Moz Au and 12.1 Moz Ag were produced between 1987 and 2005 inclusive (Christie et al., 2007). Epithermal Au-Ag mineralization occurs in steeply dipping quartz veins that generally fill normal faults opened by dip-slip movement in an extensional regime (Spörli et al., 2006, and references therein). Veins formed prior to 10 Ma variably strike northwest to northeast, whereas younger veins generally strike northeast (Christie et al., 2007). The deposits occur in the central part of alteration aureoles that are 10 to 50 km^2 in size, in which volcanic rocks are intensely altered to an association of quartz, chlorite, illite, and pyrite, with or without adularia, albite, and calcite (Christie et al., 2007, and references therein).

Geology of the Waitekauri Area

In the southern Hauraki goldfield, a ~20-km^2 magnetic quiet zone envelops epithermal deposits and prospects in the Waitekauri-Maratoto area and defines an area where magnetite has been destroyed by alteration. A ~24-km^2 zone of rocks with elevated K/Th overlaps with the magnetic quiet zone and represents the extent of rocks that experienced K metasomatism (Morrell et al., 2011). This geophysically defined alteration zone corresponds closely to a geologically defined alteration zone mapped by Brathwaite and Christie (1996). The deposits within the alteration zone have nonoverlapping $^{40}Ar/^{39}Ar$ ages (Golden Cross: 6.98 ± 0.11 Ma, Sovereign: 6.81 ± 0.06 to 6.56 ± 0.08 Ma, Maratoto: 6.41 ± 0.04 Ma, Komata: 6.06 ± 0.06 Ma), indicating that the altered zone includes separate hydrothermal alteration aureoles that overlap spatially to produce a large contiguous alteration zone (Mauk et al., 2011; Morrell et al., 2011).

The altered rock sample set on which this paper is based comprises rocks of the Waitekauri area, which forms the southern half (12.7 km^2) of the Waitekauri-Maratoto area and contains the historic workings of the Sovereign, Jubilee, and Scotia deposits, and the Jasper Creek, Scimitar and Teutonic prospects (Simpson and Mauk, 2011). Prior to 1930, the Sovereign, Jubilee, and Scotia deposits produced 392 kg Au-Ag bullion, with 78 percent mined from Jubilee (Downey, 1935). These deposits and prospects occur in altered Coromandel Group rocks of the Waipupu Formation and the Mangakara and Waitekauri Dacites (Fig. 1C). The Waipupu Formation consists of lava flows and breccias of porphyritic plagioclase + hypersthene + augite andesite and dacite, locally with quartz or resorbed hornblende. Potassium-argon ages range between 7.9 and 6.3 Ma, however, only the older ages are geologically plausible eruption ages (Brathwaite and Christie, 1996). The Waipupu Formation is the main host rock at Sovereign, Jasper Creek, and at depth at Scotia. The Mangakara Dacite overlies the Waipupu Formation and comprises porphyritic plagioclase + quartz + pyroxene + hornblende lava flows that host the Teutonic prospect. A single K-Ar date indicates a minimum age of 6.9 ± 0.5 Ma (Brathwaite and Christie, 1996). The Waitekauri Dacite overlies both the Waipupu Formation and the Mangakara Dacite and is inferred to be similar in age to the latter. It is the main host rock at the Scotia and Jubilee deposits and comprises plagioclase + hornblende + pyroxene + quartz lava flows. In addition, altered dikes of the Maratoto Rhyolite occur locally in drill core, underground, and at the surface, predominantly at

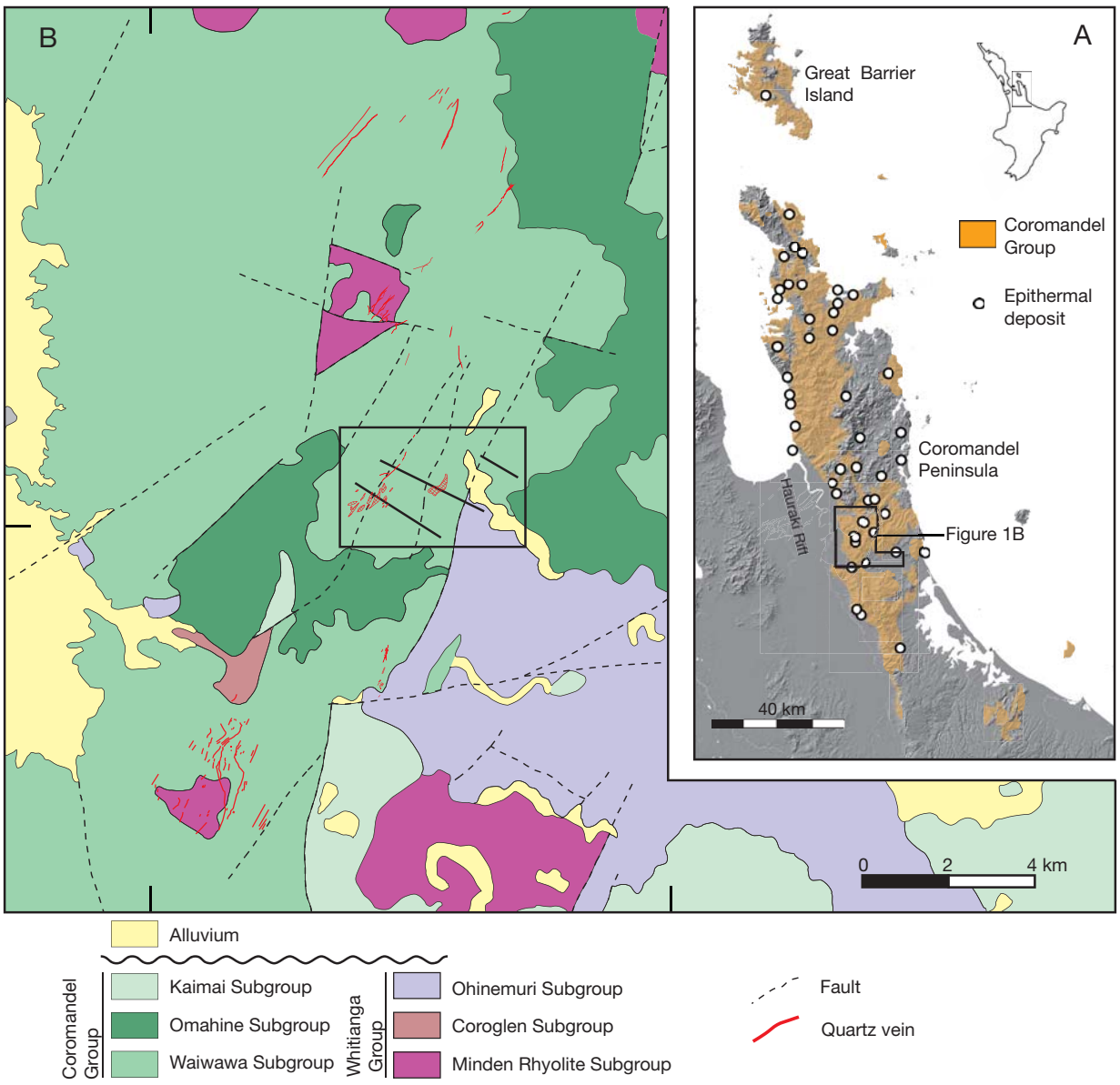

FIG. 1. A. Map of the Hauraki goldfield, showing the distribution of the Coromandel Group and the location of known mineralization occurrences. Modified after Edbrooke (2001). B. Geologic map of the southern Coromandel peninsula modified after Brathwaite and Christie (1996). The box indicates the position of (C). C. Geologic map of the Waitekauri area, showing the position of the Jasper Creek, Jubilee-Scotia, and Sovereign-Scimitar-Teutonic cross sections and the locations of drill holes. D. Geologic cross sections. Several drill holes protrude above the cross-section topographic surface due to having been projected up to 100 m onto the section. Map and sections based on unpublished mapping by Newmont Mining Corporation, after Simpson and Mauk (2011).

Jubilee (Haworth and Briggs, 2006). On the flanks of the Waitekauri Valley, these older formations are overlain by younger, unaltered Whakamoehau Andesite, which has K-Ar dates of 6.7 and 6.6 Ma (Brathwaite and Christie, 1996). Northeast-striking faults dominate the structure and include the major Waitekauri fault (Fig. 1C-D; Grodzicki et al., unpub. data). The Sovereign and Jubilee deposits occur to the east and west of the Waitekauri fault, respectively, whereas Scimitar, Scotia, Teutonic, and Jasper Creek are located progressively farther to the east (Fig. 1C).

Simpson and Mauk (2011) provide detailed descriptions of the nature and distribution of the alteration mineralogy; we provide a summary here. Host rocks in the Waitekauri area are typically intensely altered, with 100 percent of igneous minerals replaced at Sovereign, Jubilee, Scotia, and Scimitar. The alteration intensity is more variable on the eastern margin of Scotia and Scimitar, as well as at Teutonic and in the deepest drill hole at Jasper Creek, and is characterized by moderately to weakly altered rocks where 20 to 50 percent of the igneous minerals have been replaced by hydrothermal minerals. Moderately altered rocks show partial replacement of plagioclase and magnetite and complete replacement of mafic minerals and groundmass interstitial glass. In weakly altered rocks in which less than 20 percent of igneous minerals

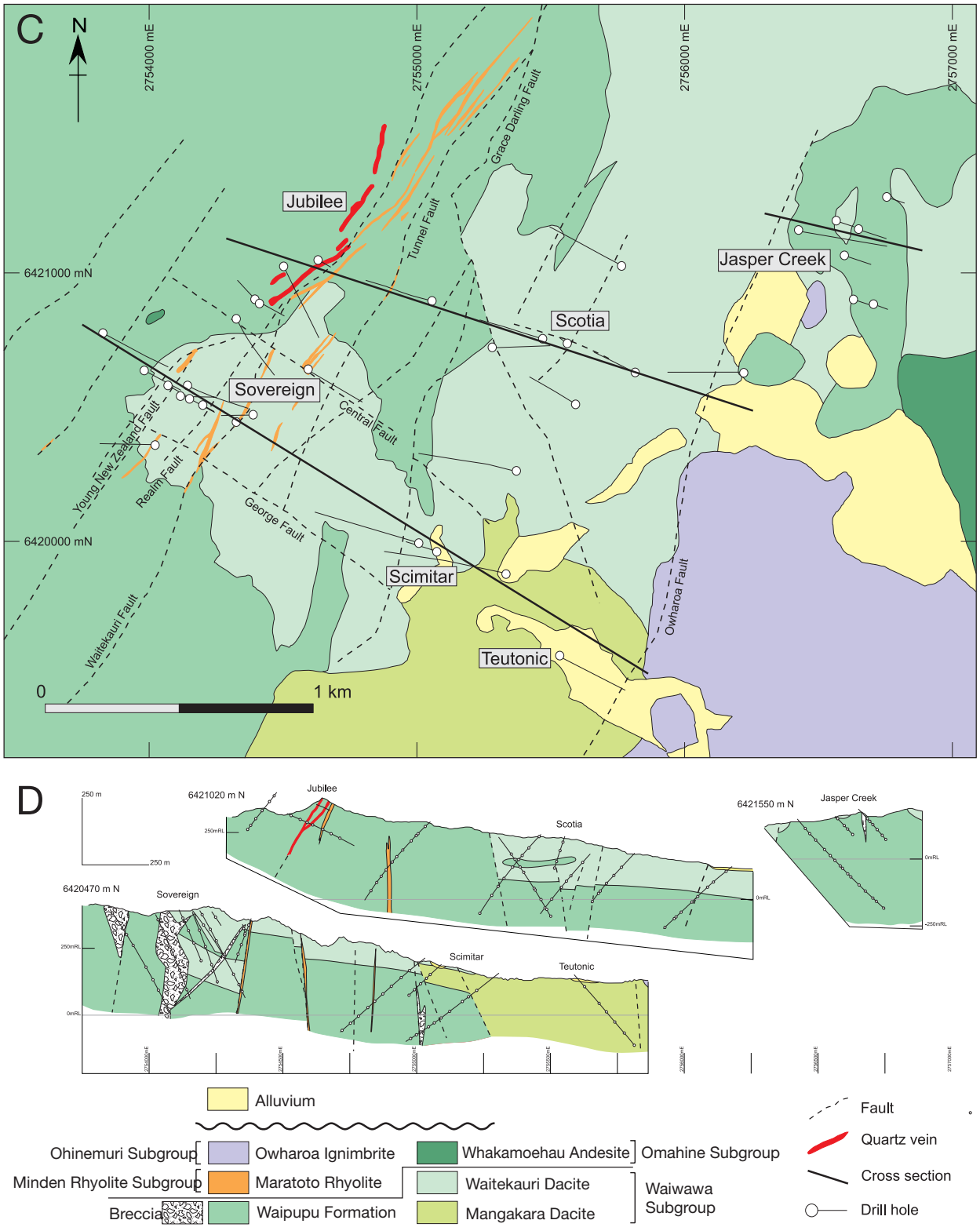

FIG. 1. *(Cont.)*

are replaced by alteration minerals, augite and some hypersthene are partially preserved, and plagioclase and magnetite are essentially unaltered. The common alteration minerals in host rocks are quartz (SiO_2), adularia ($KAlSi_3O_8$), illite (e.g., K mica, $KAl_3Si_3O_{10}(OH)_2$), smectite ($(Na,Ca)_{0.33}(Al,Mg)_2Si_4O_{10}(OH)_2{\cdot}nH_2O$), interstratified illite-smectite, chlorite (e.g., $(Mg,Fe^{2+})_5Al_2Si_3O_{10}(OH)_8$), calcite ($CaCO_3$), and pyrite ($FeS_2$), with minor albite ($NaAlSi_3O_8$) and rare epidote,

hematite, corrensite, and chlorite-smectite. Petrographic data indicate that adularia and albite were among the first alteration minerals to form. Illite invariably replaces adularia; calcite commonly occurs as a late replacement mineral that overprints adularia and illite. The dominant clay species in altered host rocks is illite at Jubilee, westernmost Scimitar, and Sovereign; interstratified illite-smectite at Scotia and Scimitar; and smectite at Jasper Creek and Teutonic. Quartz is dominant in epithermal veins at Sovereign and Jubilee and also occurs in stockwork veins at Scotia, whereas calcite is more abundant in veins at Scotia, Scimitar, and Jasper Creek. Fluid inclusions trapped in quartz and calcite yield homogenization temperatures of ca. 240°C at Sovereign, Jubilee, and Scimitar, 204°C at Scotia, and ca. 165°C at Teutonic and Jasper Creek (Simpson and Mauk, 2011).

Sample Selection and Analytical Methods

The altered-rock sample set on which this paper is based comprises 127 altered rocks that were chemically analyzed, selected from a suite of 225 rocks whose alteration mineralogy was studied in detail. The samples are spaced at approximately 50- to 100-m intervals in drill cores obtained by Newmont Mining Corporation along west-northwest–striking transects that stretch from the Waitekauri fault to the eastern edge of the Waitekauri area alteration zone. This study only determined the geochemistry of altered host rocks, and we avoided inclusion of veins, which typically host Au-Ag mineralization and pathfinder elements such as As, Sb, and Hg. This approach differs from standard industry practice, which determines total grade over a specified interval including veins and makes it possible to directly compare the geochemistry of altered host rocks to that of unaltered equivalent rocks.

Unaltered Coromandel Group volcanic rocks (n = 98) were selected from collections at the University of Auckland and at GNS Science. These were originally collected and petrographically described for mapping and research. All samples are lavas because these are the freshest, best preserved rocks, and represent massive flows, breccias, dikes, and massive boulders in reworked deposits. For all rocks, 100 to 150 g was pulverized in a tungsten-carbide ring mill. Major element concentrations were determined on fused glass beads at the University of Auckland. For major elements the analytical precision error is negligible compared to the reproducibility of the sample splitting process, which is better than 1 percent based on repeat analyses of three internal standard reference powders. Trace element ICP-MS analyses were performed by ALS Chemex in Vancouver, Canada. The concentrations of trace elements other than Hg and Au were determined in solution by ICP-MS following near-total digestion by hydrochloric, nitric, perchloric, and hydrofluoric acids of powdered sample aliquots. Mercury concentration was determined by cold vapor atomic absorption spectrometry following aqua regia digestion and Au concentration by atomic absorption spectrometry following fire assaying. Reproducibility, including sample splitting, is better than 10 percent for most trace elements. Following standard practice we report major elements (Na, Mg, Al, Si, P, K, Ca, Ti, Mn, Fe) as their respective oxides (Na_2O, MgO, Al_2O_3, SiO_2, P_2O_5, K_2O, CaO, TiO_2, MnO, Fe_2O_3). Fe_2O_3 represents total iron oxide because the analyses were performed on oxidized material. Major element oxide concentration totals were greater than 97 percent except in some samples with a high S concentration. The mineralogy of the altered rocks was qualitatively determined using X-ray diffraction for which procedures and results are described in Simpson and Mauk (2011). Representative chemical analyses of altered rocks from the Waitekauri area are listed in Table 1. The full data set is available on request. The unaltered rock data set forms the basis of an upcoming paper on the volcanic development of the Hauraki volcanic region.

Geochemistry of Unaltered Coromandel Group Rocks

Unaltered Coromandel Group rocks have 53 to 63 percent SiO_2 and are basaltic andesite, andesite, and dacite following the IUGS total alkali classification (Le Bas et al., 1986; Fig. 2A) of medium K composition (classification of Gill 1981; Fig. 2B). Normalized trace element distributions show distinct negative anomalies for the high field strength elements Nb, Ta, and Ti, which is typical of subduction-related volcanic rocks (Fig. 2C). The samples form an array in terms of major element composition, where SiO_2 concentration correlates with the concentrations of many other elements. K_2O, Rb, and Ba correlate positively with SiO_2; Na_2O, Zr, and Tl correlate

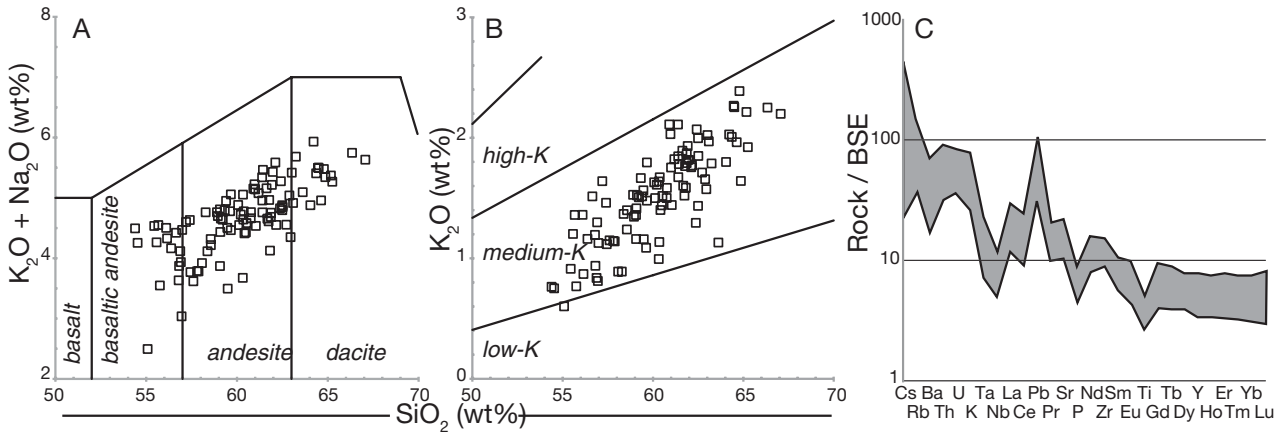

FIG. 2. Geochemistry of unaltered Coromandel Group rocks (n = 98). A. Total alkali-silica classification following Le Bas et al. (1986). B. Potassium-silica classification diagram following Gill (1981). C. Bulk silicate earth (BSE) normalized minor and trace element distribution diagram using the model BSE composition of Sun and McDonough (1989).

TABLE 1. Representative Geochemical Analyses of the Waitekauri Area Altered Rocks[1]

	Jubilee						
AU no.	AU59868	AU59878	AU59845		AU59847	AU59850	AU59858
Core-depth (m)	WV06-154	WV06-351	WV07-050	WV07-095	WV07-135	WV08-020	WV08-246
SiO_2	63.40	71.47	64.21	62.95	67.13	58.60	61.34
TiO_2	0.54	0.63	0.65	0.59	0.43	0.83	0.97
Al_2O_3	15.12	15.02	15.80	15.85	14.85	20.01	17.31
Fe_2O_3	6.21	2.63	6.00	5.37	4.01	9.49	8.51
MnO	0.49	0.06	0.10	0.11	0.08	0.09	0.07
MgO	3.86	4.62	4.28	2.80	1.82	2.88	5.35
CaO	2.92	0.36	3.78	6.89	3.41	1.17	0.40
Na_2O	0.00	0.00	0.04	1.40	2.98	0.08	0.75
K_2O	3.71	3.50	2.54	2.59	2.87	4.41	3.96
P_2O_5	0.10	0.11	0.04	0.11	0.09	0.15	0.14
Total oxides	**96.35**	**98.40**	**97.44**	**98.66**	**97.67**	**97.71**	**98.80**
Li	48.4	97.7	112.0	54.6	44.6	35.2	110.0
Be	0.81	1.06	0.87	0.60	1.03	0.78	0.96
S (%)	2.57	1.34	0.94	0.06	0.35	6.48	0.10
Sc	18	26	27	19	14	38	35
V	130	150	170	127	77	285	260
Cr	217	134	114	44	30	108	86
Co	22.4	19.8	22.3	20.1	18.0	47.8	30.6
Ni	20	31	54	9	10	33	30
Cu	10	5	19	10	6	284	28
Zn	47	22	71	50	37	47	93
Ga	16	15	16	15	13	22	18
Ge	0.16	0.13	0.15	0.14	0.14	0.24	0.18
As	31.6	6.2	79.3	5.4	2.7	61.6	3.7
Se	3	3	3	2	2	17	3
Rb	177	165	143	129	104	283	205
Sr	24	14	40	68	152	52	72
Y	24	22	28	20	20	34	37
Zr	144	139	144	117	133	114	105
Nb	6	6	5	5	6	5	5
Mo	1.19	63.10	5.73	0.59	0.87	2.41	0.14
Ag	0.34	0.80	0.13	0.05	0.06	0.45	0.07
Cd	0.05	<0.02	0.05	0.09	0.02	0.11	0.05
In	0.040	0.027	0.038	0.030	0.025	0.321	0.043
Sn	1.3	7.4	1.3	1.0	1.1	2.1	1.0
Sb	5.66	0.48	2.08	0.80	0.48	6.61	1.85
Te	0.61	0.44	0.05	<0.05	<0.05	0.72	<0.05
Cs	9.25	7.05	9.12	5.31	6.18	15.80	15.40
Ba	676	254	369	383	810	441	347
La	13	9	11	13	15	9	17
Ce	24	28	29	30	29	27	32
Hf	0.9	1.3	3.5	2.3	1.7	1.3	2.5
Ta	0.46	0.38	0.42	0.42	0.52	0.28	0.35
Re	<0.002	1.375	<0.002	<0.002	<0.002	0.194	<0.002
Au	<0.005	0.009	0.065	<0.005	<0.005	<0.005	<0.005
Hg	0.01	<0.01	0.01	0.01	0.01	0.05	0.01
Tl	1.73	1.78	1.44	1.05	0.80	2.55	1.78
Pb	10	6	3	9	9	16	7
Bi	0.01	0.54	0.69	0.03	0.02	3.01	0.02
Th	7.1	4.8	6.8	5.8	8.9	5.6	4.3
U	2.2	0.3	2.0	1.3	2.9	0.0	0.7
Molar K/Al	0.27	0.25	0.17	0.18	0.21	0.24	0.25
Molar (K+Na+2Ca)/Al	0.62	0.30	0.61	1.11	0.96	0.35	0.36
Molar K/(K+Na+2Ca)	0.43	0.85	0.28	0.16	0.22	0.68	0.69
$100/Zr/TiO_2$	2.67	2.21	2.22	1.97	3.08	1.38	1.08
Easting (m)	2754951	2754833	2754390	2754364	2754341	2754516	2754671
Northing (m)	6420933	6420974	6420910	6420923	6420934	6421018	6420876
Elevation (m asl)	183	30	362	328	297	315	230

TABLE 1. *(Cont.)*

	Scotia								
AU no.	AU59882	AU59895	AU59915	AU59919	AU59924			AU59911	AU59930
Core-depth (m)	SC27-082	SC27-356	SC28-048	SC28-175a	SC33-164	SC33-202	SC33-253	SC36-026	WV02-036
SiO_2	66.84	62.08	72.19	64.44	64.15	62.15	59.71	65.83	68.05
TiO_2	0.49	0.68	0.47	0.57	0.57	0.81	0.89	0.53	0.58
Al_2O_3	14.51	16.55	13.57	16.67	16.49	17.86	19.45	20.79	16.44
Fe_2O_3	4.97	5.84	2.56	5.06	5.03	6.95	9.03	0.74	4.17
MnO	0.06	0.09	0.01	0.10	0.07	0.11	0.12	0.00	0.03
MgO	3.70	2.26	0.66	2.61	2.21	3.17	3.74	0.10	2.28
CaO	0.37	4.50	0.34	3.67	3.61	2.73	3.79	0.17	1.77
Na_2O	0.14	2.54	0.33	2.14	0.53	2.19	1.34	0.40	2.00
K_2O	6.89	2.94	8.09	2.81	5.07	2.37	0.94	9.35	2.81
P_2O_5	0.09	0.13	0.09	0.10	0.11	0.14	0.14	0.30	0.11
Total oxides	**98.06**	**97.61**	**98.31**	**98.17**	**97.84**	**98.48**	**99.15**	**98.21**	**98.24**
Li	91.0	88.4	66.0	95.9	90.0	103.5	81.9	25.4	102.0
Be	0.87	1.18	0.94	0.97	0.97	1.22	1.16	0.92	1.04
S (%)	1.05	0.71	1.51	0.19	0.53	0.09	<0.01	1.03	0.59
Sc	21	24	21	20	25	27	36	21	22
V	134	145	112	133	151	171	187	125	133
Cr	85	42	82	135	147	107	72	61	147
Co	21.6	21.2	43.2	17.8	27.3	25.0	29.7	8.0	18.4
Ni	19	12	13	17	20	16	18	37	16
Cu	7	17	10	15	16	22	16	9	12
Zn	47	59	50	59	61	82	75	9	40
Ga	15	17	13	16	16	17	18	16	16
Ge	0.14	0.16	0.11	0.14	0.14	0.17	0.18	0.15	0.12
As	151.0	86.6	192.0	13.3	78.9	2.3	1.4	364.0	30.6
Se	2	2	2	1	2	2	2	2	2
Rb	288	106	358	104	220	123	39	354	145
Sr	103	260	166	261	123	215	186	381	214
Y	29	26	24	20	25	25	22	37	18
Zr	118	140	108	127	119	141	126	142	122
Nb	5	6	5	5	5	6	5	7	5
Mo	0.12	0.47	0.87	0.09	0.46	0.15	0.22	0.38	0.16
Ag	0.46	0.18	0.69	0.07	0.42	0.05	0.05	0.63	0.11
Cd	<0.02	0.03	0.02	0.06	0.05	0.03	0.04	<0.02	<0.02
In	0.026	0.034	0.023	0.036	0.037	0.038	0.067	0.026	0.032
Sn	0.6	1.3	0.7	1.2	1.0	1.3	1.4	1.0	1.0
Sb	3.24	2.30	14.15	1.94	3.42	1.52	0.41	12.25	3.91
Te	<0.05	<0.05	<0.05	<0.05	<0.05	<0.05	<0.05	<0.05	<0.05
Cs	6.30	8.43	11.50	5.89	14.05	16.80	8.71	6.78	16.00
Ba	765	778	504	588	827	301	257	1244	180
La	14	12	9	14	13	14	9	17	11
Ce	37	34	32	28	30	38	28	40	32
Hf	1.0	3.0	0.9	2.0	1.6	3.1	2.6	1.5	2.1
Ta	0.41	0.48	0.45	0.45	0.43	0.45	0.38	0.54	0.39
Re	<0.002	<0.002	0.003	<0.002	<0.002	<0.002	<0.002	<0.002	<0.002
Au	0.146	0.018	0.031	<0.005	0.018	0.006	<0.005	0.063	0.006
Hg	0.01	0.01	0.71	0.06	0.25	0.01	<0.01	0.48	0.04
Tl	4.21	1.20	5.85	1.00	2.91	1.04	0.24	5.53	0.94
Pb	7	9	6	10	6	11	8	9	7
Bi	0.01	0.00	0.00	0.08	0.04	0.01	0.05	0.03	0.02
Th	6.4	5.0	5.9	8.3	6.5	5.2	5.1	8.1	6.5
U	0.6	1.9	0.0	1.9	0.8	1.9	2.3	0.0	2.6
Molar K/Al	0.51	0.19	0.65	0.18	0.33	0.14	0.05	0.49	0.19
Molar (K+Na+2Ca)/Al	0.58	0.94	0.73	0.79	0.78	0.62	0.52	0.53	0.58
Molar K/(K+Na+2Ca)	0.89	0.20	0.88	0.23	0.42	0.23	0.10	0.91	0.32
$100/Zr/TiO_2$	2.40	2.05	2.29	2.22	2.09	1.74	1.41	2.68	2.10
Easting (m)	2755335	2755494	2755564	2755490	2755712	2755690	2755662	2755555	2756191
Northing (m)	6420727	6420732	6420533	6420578	6420684	6420695	6420708	6420747	6420630
Elevation (m asl)	169	-54	135	42	56	27	-12	211	102

TABLE 1. *(Cont.)*

	Scotia			Jasper Creek				
AU no.	AU59935	AU59898	AU59910	AU59981	AU59973	AU59987	AU59956	AU59968
Core-depth (m)	WV02-276	WV04-073	WV04-385	JC15-156	JC17-096	JC20-052	WV09-208	WV09-466
SiO_2	67.38	72.42	57.02	64.02	65.53	73.19	63.60	68.85
TiO_2	0.48	0.56	0.74	0.58	0.56	0.57	0.52	0.51
Al_2O_3	14.42	17.08	16.68	16.57	16.15	14.07	15.03	15.19
Fe_2O_3	3.26	2.03	7.19	5.71	4.65	4.30	5.27	4.34
MnO	0.05	0.03	0.15	0.10	0.07	0.03	0.12	0.10
MgO	1.50	0.87	5.04	2.90	3.24	2.37	3.12	2.14
CaO	5.39	0.81	6.94	5.21	4.24	0.79	6.38	4.30
Na_2O	1.43	0.00	0.79	0.49	0.06	0.03	2.51	0.93
K_2O	2.36	4.63	3.20	3.26	3.55	3.29	2.35	2.25
P_2O_5	0.10	0.03	0.15	0.10	0.10	0.09	0.10	0.10
Total oxides	**96.37**	**98.46**	**97.90**	**98.94**	**98.15**	**98.73**	**99.00**	**98.71**
Li	97.3	67.6	74.5	89.0	155.5	110.0	27.2	29.5
Be	1.03	1.20	0.96	0.93	0.87	1.07	0.80	0.86
S (%)	0.04	0.52	1.40	<0.01	0.55	1.17	<0.01	0.33
Sc	22	19	27	21	21	21	21	15
V	108	162	172	42	135	76	96	94
Cr	92	96	86	41	66	18	78	84
Co	15.0	23.0	24.0	19.5	18.4	14.8	20.5	14.3
Ni	14	17	26	13	16	6	16	10
Cu	7	9	25	13	15	2	17	8
Zn	32	49	77	45	46	52	49	36
Ga	14	18	16	15	16	14	14	14
Ge	0.16	0.13	0.16	0.16	0.12	0.11	0.14	0.14
As	3.9	128.0	6.9	1.9	66.7	232.0	2.4	75.8
Se	2	2	2	2	1	2	2	3
Rb	106	230	150	120	129	181	66	74
Sr	150	51	92	182	149	52	199	95
Y	20	21	21	20	21	23	19	18
Zr	112	119	115	114	109	109	95	110
Nb	5	6	5	5	5	6	4	4
Mo	0.19	0.30	0.67	<0.05	0.38	0.19	0.24	0.78
Ag	0.03	0.03	0.41	0.03	0.83	0.11	0.03	0.03
Cd	<0.02	0.15	0.02	0.04	0.04	0.05	0.13	0.02
In	0.025	0.035	0.034	0.028	0.033	0.023	0.037	0.019
Sn	0.7	1.1	1.1	0.9	1.2	1.0	1.6	1.0
Sb	1.34	26.90	1.34	6.74	8.83	13.45	0.33	6.42
Te	<0.05	<0.05	0.10	<0.05	<0.05	<0.05	<0.05	<0.05
Cs	10.85	24.20	7.36	37.50	16.20	16.70	1.88	5.30
Ba	388	925	341	761	429	453	598	530
La	14	13	12	14	10	15	9	13
Ce	23	38	30	23	31	36	28	35
Hf	0.8	1.6	2.0	2.1	1.9	2.0	2.5	1.3
Ta	0.47	0.48	0.36	0.41	0.36	0.39	0.35	0.42
Re	<0.002	<0.002	<0.002	<0.002	<0.002	<0.002	<0.002	<0.002
Au	<0.005	<0.005	<0.005	0.008	0.055	0.015	<0.005	<0.005
Hg	0.01	1.12	0.09	0.04	0.33	0.09	<0.01	0.23
Tl	0.60	6.45	1.58	0.57	2.09	1.50	0.34	0.31
Pb	5	10	8	7	6	8	8	8
Bi	0.01	0.02	0.03	0.03	0.19	0.02	0.00	0.01
Th	7.0	8.1	3.5	6.7	6.4	5.3	6.0	7.3
U	1.8	1.9	1.3	2.2	2.1	1.2	2.7	3.6
Molar K/Al	0.18	0.29	0.21	0.21	0.24	0.25	0.17	0.16
Molar (K+Na+2Ca)/Al	1.02	0.38	1.04	0.83	0.72	0.36	1.22	0.78
Molar K/(K+Na+2Ca)	0.17	0.77	0.20	0.26	0.33	0.71	0.14	0.21
$100/Zr/TiO_2$	2.34	2.13	1.55	1.97	1.95	1.92	1.83	2.15
Easting (m)	2756005	2755421	2755236	2756753	2756630	2756665	2756561	2756745
Northing (m)	6420633	6420774	6420830	6421126	6421172	6420888	6421126	6421098
Elevation (m asl)	-51	190	-55	74	93	94	-5	-182

TABLE 1. *(Cont.)*

	Sovereign												
AU no.	AU59767	AU59751	AU59754	AU59737	AU59745	AU59727	AU59730	AU59765	AU59762	AU59746	AU59748	AU59757	AU59760
Core-depth (m)	ML01-027	ML11-147	ML11-293	ML12-022	ML12-315	ML13-017	ML13-171	ML23-017	ML06-085	ML07-036	ML07-142	WV01-225	WV01-382
SiO_2	76.93	61.10	66.14	65.34	64.51	50.36	62.54	78.15	63.28	67.91	70.61	77.88	60.39
TiO_2	0.23	0.88	0.72	0.71	0.76	1.08	0.72	0.17	0.84	0.68	0.62	0.31	0.75
Al_2O_3	13.40	20.13	15.75	15.84	17.76	27.46	16.94	12.46	17.26	19.93	14.34	10.82	15.07
Fe_2O_3	1.53	7.84	6.34	6.28	6.72	9.71	7.31	6.43	6.71	3.41	4.51	1.89	7.31
MnO	0.00	0.14	0.10	0.09	0.08	0.07	0.05	0.00	0.13	0.01	0.05	0.01	0.12
MgO	0.19	3.78	3.31	2.44	3.47	8.64	2.89	0.07	1.84	0.78	1.99	0.59	4.44
CaO	0.01	0.22	0.22	0.06	0.32	0.67	0.69	0.00	0.12	0.01	0.04	0.12	5.73
Na_2O	0.01	0.06	0.02	0.05	0.02	0.19	2.88	0.00	0.07	0.00	0.01	0.01	1.11
K_2O	6.86	5.03	6.04	8.07	5.09	0.96	4.97	1.94	8.76	5.66	6.66	7.36	2.25
P_2O_5	0.02	0.14	0.13	0.06	0.16	0.20	0.11	0.13	0.09	0.12	0.06	0.09	0.14
Total oxides	**99.18**	**99.31**	**98.78**	**98.95**	**98.88**	**99.34**	**99.09**	**99.36**	**99.10**	**98.51**	**98.89**	**99.07**	**97.32**
Li	11.4	77.8	65.8	56.3	49.9	243.0	59.1	19.4	41.2	9.0	44.8	28.7	100.5
Be	0.90	1.20	1.19	0.60	0.98	1.44	0.80	0.44	0.76	0.83	0.99	0.57	0.71
S (%)	0.01	0.17	2.13	2.31	3.63	0.05	3.83	0.02	0.51	1.93	1.70	1.03	1.01
Sc	6	31	30	27	27	37	29	2	35	30	24	12	28
V	22	223	216	201	181	178	175	16	277	194	198	84	210
Cr	5	168	94	60	79	58	167	7	87	315	139	34	92
Co	19.9	25.9	24.7	24.3	25.0	24.1	35.8	24.4	29.4	52.1	24.5	51.9	31.0
Ni	2	27	17	28	26	32	66	4	25	97	23	9	26
Cu	3	14	9	17	17	15	37	17	20	30	33	8	10
Zn	7	137	58	93	58	131	78	13	84	46	56	30	63
Ga	13	19	16	17	18	22	15	7	17	16	14	9	16
Ge	0.07	0.09	0.11	0.09	0.1	0.1	0.11	0.1	0.11	0.16	0.13	0.11	0.13
As	176.0	27.6	44.6	127.0	20.1	1.2	13.2	364.0	48.7	93.2	273.0	181.5	25.3
Se	2	2	2	2	2	2	1	1	1	4	2	2	2
Rb	297	243	278	325	226	42	190	80	353	303	273	292	108
Sr	55	35	68	55	32	33	180	22	93	76	66	70	56
Y	27	30	26	24	23	81	22	8	25	154	32	22	20
Zr	124	149	98	108	118	192	111	88	101	134	88	71	105
Nb	7	7	6	5	6	8	5	5	6	7	5	5	5
Mo	1.24	0.58	0.92	0.95	0.69	0.06	1.59	1.17	0.26	0.48	2.25	5.07	0.75
Ag	0.60	0.07	0.89	1.04	0.89	0.07	1.77	0.37	0.77	1.46	0.96	1.46	0.74
Cd	0.02	0.09	0.03	0.05	0.02	0.07	0.11	0.02	0.06	0.12	0.17	0.11	0.02
In	0.020	0.050	0.047	0.050	0.043	0.058	0.045	0.020	0.048	0.040	0.035	0.020	0.045
Sn	1.5	1.3	1.1	1.0	1.1	1.9	1.1	0.7	1.3	1.3	1.2	1.3	1.3
Sb	7.40	4.67	3.64	2.93	2.98	0.50	3.11	18.05	3.16	3.28	6.38	15.65	2.08
Te	0.05	0.05	0.23	0.05	0.62	0.05	0.11	1.59	0.05	0.06	0.11	0.05	0.05
Cs	5.32	17.15	12.40	6.73	8.69	5.20	4.42	1.83	7.67	12.95	7.49	7.00	5.27
Ba	558	248	804	536	526	129	463	144	412	676	723	683	274
La	16	14	11	7	11	33	7	21	11	30	18	14	10
Ce	35	40	23	22	21	74	21	56	24	71	41	31	28
Hf	1.8	2.6	1.5	1.2	1.3	4.9	1.3	1.2	1.8	1.4	1.3	1.6	1.7
Ta	0.63	0.43	0.38	0.25	0.36	0.51	0.31	0.50	0.45	0.34	0.42	0.47	0.37
Re	0.003	0.002	0.002	0.002	0.002	0.002	0.006	0.002	0.002	0.004	0.002	0.004	0.002
Au	0.230	0.005	0.008	0.059	0.009	0.005	0.012	0.401	0.020	0.023	0.131	0.131	0.005
Hg	0.07	0.06	0.08	0.08	0.03	0.04	0.17	0.16	0.09	0.07	0.05	0.33	0.05
Tl	4.92	2.43	3.40	5.86	2.09	0.43	2.39	1.41	4.70	3.45	3.27	4.92	0.94
Pb	6	6	11	5	18	3	15	46	8	14	9	13	7
Bi	0.01	0.03	0.08	0.08	0.51	0.01	0.07	0.01	0.04	0.48	0.02	0.15	0.14
Th	12.7	6.9	6.3	3.4	3.9	6.9	4.2	9.9	7.6	4.5	5.8	8.9	3.4
U	1.4	0.3	0.0	0.0	0.5	3.8	0.7	3.5	1.3	0.0	1.4	1.8	2.0
Molar K/Al	0.55	0.27	0.42	0.55	0.31	0.04	0.32	0.17	0.55	0.31	0.50	0.74	0.16
Molar (K+Na+2Ca)/Al	0.56	0.29	0.44	0.56	0.34	0.09	0.67	0.17	0.57	0.31	0.51	0.76	0.97
Molar K/(K+Na+2Ca)	0.99	0.92	0.94	0.98	0.90	0.40	0.47	1.00	0.97	1.00	0.99	0.97	0.17
$100/Zr/TiO_2$	5.47	1.70	1.35	1.51	1.55	1.78	1.53	5.08	1.20	1.97	1.41	2.26	1.39
Easting (m)	2754379	2754194	2754267	2753996	2754123	2753843	2753928	2754334	2754197	2754091	2754137	2754037	2753954
Northing (m)	6420481	6420548	6420544	6420643	6420570	6420783	6420734	6420452	6420519	6420583	6420556	6420659	6420698
Elevation (m asl)	336	256	124	356	95	382	261	324	321	263	269	219	88

TABLE 1. *(Cont.)*

	Scimitar						Teutonic			
AU no.	AU59791	AU59802	AU59805	AU59810	AU59821	AU59833			AU59842	AU59824
Core-depth (m)	WV11-089	WV11-477	WV12-086	WV15-125	WV15-501	WV10-067	WV10-157	WV10-258	WV10-383	WV14-141
SiO_2	79.25	59.45	72.54	63.47	58.04	71.68	68.50	71.08	73.72	66.71
TiO_2	0.22	0.92	0.53	0.73	0.90	0.43	0.44	0.49	0.43	0.53
Al_2O_3	14.12	19.02	15.59	19.55	19.09	14.37	14.72	15.65	14.44	15.71
Fe_2O_3	0.96	6.24	3.94	6.77	10.29	4.09	3.88	3.51	2.65	4.80
MnO	0.01	0.12	0.01	0.09	0.16	0.05	0.12	0.04	0.04	0.09
MgO	0.61	2.48	1.06	2.34	3.22	1.15	1.16	0.71	0.80	3.01
CaO	0.14	2.87	0.30	2.30	1.69	2.55	4.08	2.25	3.05	4.38
Na_2O	0.07	0.10	0.11	0.51	3.92	2.46	2.75	2.29	1.72	2.51
K_2O	3.71	5.34	5.64	3.02	2.19	2.89	2.82	3.06	2.49	2.19
P_2O_5	0.02	0.16	0.11	0.08	0.17	0.08	0.09	0.10	0.09	0.10
Total oxides	**99.11**	**96.70**	**99.83**	**98.86**	**99.66**	**99.76**	**98.55**	**99.18**	**99.43**	**100.03**
Li	31.6	39.0	25.7	51.3	43.4	39.7	27.7	66.4	58.6	24.8
Be	0.81	1.15	1.18	1.16	0.82	1.34	0.96	1.16	0.81	1.10
S (%)	0.50	3.51	2.92	0.51	2.34	<0.01	<0.01	0.42	0.70	<0.01
Sc	5	21	17	20	21	12	11	11	12	16
V	19	170	126	140	181	70	76	84	73	105
Cr	3	38	73	49	36	20	24	21	15	48
Co	9.2	20.2	36.1	26.2	23.7	16.9	28.3	16.7	28.2	23.1
Ni	0	21	19	14	17	9	8	5	4	17
Cu	6	33	11	17	29	10	9	11	12	17
Zn	27	66	37	139	99	55	44	43	38	55
Ga	14	17	16	19	16	12	16	16	11	16
Ge	0.12	0.18	0.16	0.15	0.18	0.11	0.14	0.11	0.13	0.15
As	230.0	62.5	171.0	122.0	123.5	2.1	1.1	86.5	176.0	2.9
Se	2	2	2	2	2	1	1	1	1	2
Rb	173	265	303	175	104	148	106	120	98	78
Sr	17	41	36	38	294	251	165	186	174	245
Y	18	27	21	25	25	26	20	22	20	18
Zr	132	127	136	176	124	156	162	155	134	134
Nb	6	6	6	8	6	6	6	7	5	6
Mo	2.47	0.63	1.09	0.33	0.62	0.62	0.66	0.76	1.86	0.54
Ag	0.18	0.23	1.61	0.14	0.26	0.03	0.04	0.08	0.36	0.02
Cd	0.04	0.07	0.04	0.04	0.07	0.05	0.05	0.03	0.04	0.05
In	0.023	0.050	0.029	0.039	0.044	0.026	0.027	0.024	0.013	0.036
Sn	2.0	1.2	1.3	1.8	1.2	1.5	1.1	1.2	0.8	1.3
Sb	5.95	1.77	11.25	4.72	2.54	1.15	1.12	6.11	8.37	0.44
Te	<0.05	0.18	<0.05	<0.05	0.39	<0.05	<0.05	<0.05	<0.05	<0.05
Cs	8.97	17.25	13.35	24.90	6.40	7.53	5.32	9.56	17.65	3.13
Ba	198	410	647	386	220	972	640	684	493	486
La	19	11	20	23	12	23	19	23	16	21
Ce	51	35	31	33	33	47	23	35	40	35
Hf	3.4	1.8	2.2	3.2	1.4	2.1	2.1	3.7	2.3	2.6
Ta	0.69	0.39	0.46	0.53	0.40	0.54	0.53	0.57	0.50	0.50
Re	<0.002	<0.002	0.002	0.002	<0.002	0.002	<0.002	<0.002	<0.002	0.002
Au	0.115	0.035	0.040	0.034	0.049	0.026	0.024	0.012	0.081	0.008
Hg	0.07	<0.01	0.24	0.03	0.01	<0.01	<0.01	0.30	0.37	<0.01
Tl	1.93	2.61	3.94	0.98	0.89	0.39	0.33	0.53	0.39	0.31
Pb	17	11	10	11	10	19	11	12	9	12
Bi	0.18	0.05	0.06	0.05	0.03	0.03	0.04	0.06	0.01	0.08
Th	11.0	8.0	5.0	10.0	5.0	11.0	9.0	7.0	9.0	9.0
U	3.0	0.6	1.6	1.5	0.6	1.6	1.5	1.9	1.4	1.8
Molar K/Al	0.28	0.30	0.39	0.17	0.12	0.22	0.21	0.21	0.19	0.15
Molar (K+ Na+2Ca)/Al	0.31	0.59	0.44	0.42	0.62	0.82	1.02	0.71	0.77	0.92
Molar K/(K+ Na+2Ca)	0.92	0.52	0.89	0.39	0.20	0.26	0.20	0.30	0.24	0.16
$100/Zr/TiO_2$	6.00	1.38	2.57	2.41	1.38	3.63	3.68	3.16	3.12	2.53
Easting (m)	2754934	2754628	2755007	2755226	2754902	2755573	2755630	2755694	2755774	2755258
Northing (m)	6420012	6420101	6419980	6419900	6419954	6419541	6419508	6419476	6419437	6420279
Elevation (m asl)	166	-58	138	92	-88	105	43	-27	-115	99

[1] Major element and S concentrations are given in wt percent, minor and trace element concentrations in ppm; all analyses by XRF except italicized elements by ICPMS, and Au concentrations determined by fire assay

weakly positively with SiO_2; and TiO_2, Al_2O_3, Fe_2O_3, MgO, CaO, Sr, and Cu correlate negatively with SiO_2 (Table 2A). Although Na_2O and SiO_2 do not correlate strongly, Na_2O correlates strongly with MgO and Zr. The traditional "epithermal suite" pathfinder elements (e.g., As, Sb, Hg) occur at concentrations of 1 ppm or less, and Ag concentrations are about 0.1 ppm. We did not measure gold concentration in the unaltered volcanic rocks and assume it to be equal to or less than 5 ppb, which is the detection limit for Au in our altered-rock analyses.

The SiO_2-dominated compositional range in Coromandel Group rocks is typical of andesites worldwide (Gill, 1981). With increasing SiO_2 concentration, rocks become more enriched in incompatible elements, which preferentially enter or partition into the melt phase of a magma, and more depleted in compatible elements, which partition into or form the rock-forming minerals. The strong correlation of many of the major elements with each other means that the whole-rock composition of any Coromandel Group rock can be estimated with some precision if the SiO_2 concentration is known. In the next section we assess how a ratio of generally immobile elements, Zr/TiO_2, correlates with SiO_2 concentration in unaltered Coromandel Group rocks.

Zr and TiO_2 concentrations in unaltered Coromandel Group rocks

Zirconium and TiO_2 concentrations show contrasting behavior with increasing magmatic differentiation: zirconium is generally incompatible, whereas TiO_2 is compatible. TiO_2 is particularly compatible in magnetite, with partition coefficients in representative magma compositions of 4 to 8 (Shimizu and Kushiro, 1975) to 16.5 (Sisson, 1991). It is also compatible in amphibole, with partition coefficients of 2 to 4 listed by Brenan et al. (1995) and Sisson (1994). Amphibole phenocrysts are only common in rocks of pre-10 Ma formations of the Coromandel Group, but partially resorbed amphibole crystals occur in younger formations. Amphibole is likely to have been present to some extent at depth in andesitic magmas that contributed to form Coromandel Group rocks, as it is stable in hydrated magma under midcrustal conditions (Carmichael, 2002; Davidson et al., 2007). Fractionation of relatively TiO_2 rich magnetite and amphibole deplete the remaining melt in TiO_2, which is sequestered into amphibole-rich cumulates in the deep and middle crust. Titanium is not compatible in the dominant phenocryst minerals plagioclase, hypersthene, and augite (e.g., Okamoto, 1979; Johnson and Kinzler, 1989), so fractionation of those minerals increases the TiO_2 content of the melt. However, current understanding of arc volcanic systems indicates that such crystals may not control magmatic evolution and are generally not crystallization products of the associated melt (e.g. Charlier et al., 2005; Price et al., 2005). Accordingly, TiO_2 behaves as a compatible element and correlates negatively with SiO_2 in unaltered Coromandel Group rocks (Table 2, Fig. 3A).

Zirconium is moderately incompatible in pyroxene, amphibole, and magnetite, with partition coefficients in the range 0.1 to 0.9 (Ewart and Griffin, 1994). Therefore any fractionation of pyroxene, amphibole, or magnetite would enrich the melt mildly in Zr. Assimilation of a crustal partial melt might likewise only moderately enrich Zr concentration. Zirconium is more strongly incompatible in plagioclase but, as noted above, plagioclase fractionation is not a driving force for magmatic differentiation of Coromandel Group rocks. The solubility of zircon decreases in a silicate melt with decreasing temperature; the Zr concentration at which a melt of given major element composition becomes saturated in zircon can be calculated using the method of Watson and Harrison (1983). The Coromandel Group magmas, typically with 100- to 150-ppm Zr, were undersaturated in zircon even at a theoretical eruption temperature as low as 750°C. Actual eruption temperatures were probably higher than this. Consequently, Zr acted incompatibly and correlates weakly with SiO_2 in unaltered Coromandel Group rocks (Table 2, Fig. 3B).

The contrasting behavior of Zr and TiO_2 during magmatic differentiation indicates that the ratio Zr/TiO_2 must increase progressively with magmatic differentiation in arc volcanic rocks (Table 1, Fig. 3C). Because Zr is present at the 100-ppm level and TiO_2 at the percent level, we multiply all Zr/TiO_2 values by a factor of 100 to avoid long decimal numbers. Values of Zr/TiO_2 are 0.9 to 1.4 for basaltic andesite, 1.1

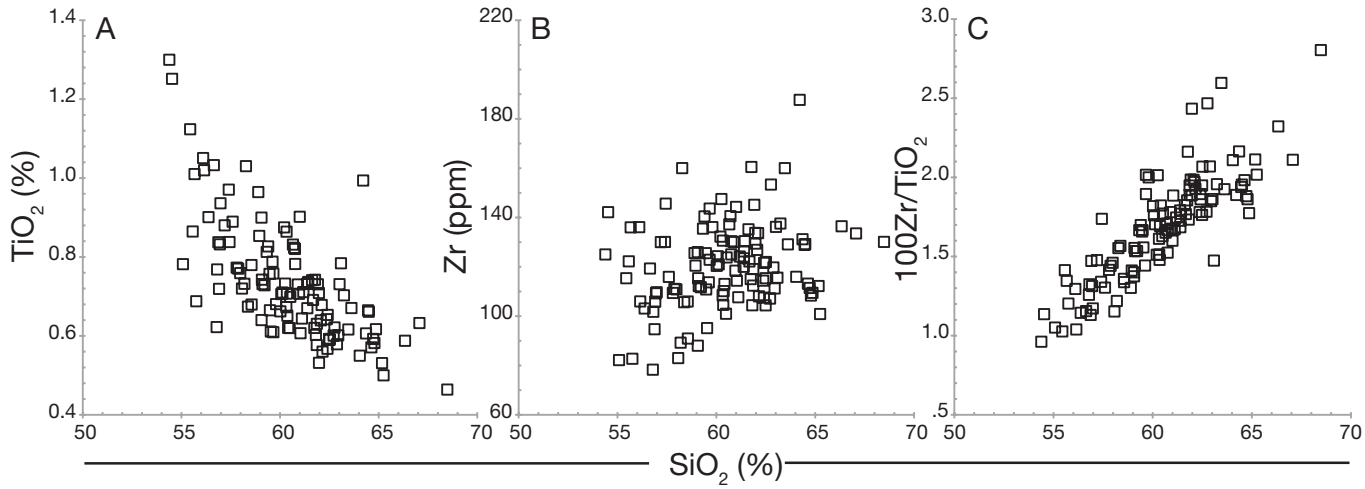

FIG. 3. Geochemistry of unaltered Coromandel Group rocks (n = 98). A. TiO_2-SiO_2. B. Zr-SiO_2. C. Zr/TiO_2-SiO_2.

TABLE 2. Correlation Coefficient Matrices for Concentrations of 18 Elements, Molar K/(K + Na + 2Ca) (noted as K#) and Zr/TiO_2

n = 98	SiO_2	TiO_2	Al_2O_3	Fe_2O_3	MgO	CaO	Na_2O	K_2O	Cu	As	Rb	Sr	Zr	Ag	Sb	Ba	Hg	Tl	K#
A. Unaltered Coromandel Group rocks																			
TiO_2	**-0.69**																		
Al_2O_3	**-0.50**	**0.65**																	
Fe_2O_3	**-0.92**	**0.75**	0.42																
MgO	**-0.70**	0.08	-0.15	**0.56**															
CaO	**-0.89**	0.41	0.22	**0.74**	**0.82**														
Na_2O	0.30	0.23	0.35	-0.25	**-0.70**	**-0.55**													
K_2O	**0.81**	-0.49	-0.41	**-0.69**	**-0.66**	**-0.81**	0.22												
Cu	-0.39	0.03	0.00	0.33	0.47	0.44	-0.30	-0.37											
As	0.06	0.06	-0.07	-0.01	-0.09	-0.04	-0.09	0.15	-0.01										
Rb	**0.77**	-0.48	-0.40	**-0.68**	**-0.59**	**-0.79**	0.24	**0.94**	-0.33	0.16									
Sr	-0.24	0.23	0.11	0.26	0.06	0.31	-0.29	-0.11	-0.03	0.24	-0.19								
Zr	0.24	0.35	0.18	-0.11	**-0.59**	-0.44	**0.54**	0.38	-0.39	0.17	0.41	0.03							
Ag	-0.12	0.09	0.13	0.12	0.01	0.07	-0.04	0.03	0.15	0.09	0.00	0.23	0.10						
Sb	0.08	-0.03	-0.08	-0.04	-0.02	-0.02	-0.25	0.07	0.02	**0.60**	0.10	0.20	0.08	0.00					
Ba	**0.77**	-0.48	-0.48	**-0.66**	**-0.55**	**-0.67**	0.07	**0.81**	-0.34	0.28	**0.77**	0.02	0.39	0.00	0.22				
Hg	-0.13	0.21	0.06	0.18	0.04	0.07	-0.01	-0.06	-0.06	-0.04	-0.05	-0.02	0.15	0.04	-0.10	-0.19			
Tl	0.36	-0.17	-0.14	-0.34	-0.29	-0.34	0.05	0.44	-0.25	0.25	**0.55**	-0.05	0.28	-0.06	0.26	0.42	-0.03		
K#	**0.87**	**-0.51**	-0.43	**-0.73**	**-0.69**	**-0.87**	0.24	**0.99**	-0.39	0.13	**0.93**	-0.14	0.36	-0.01	0.09	**0.81**	-0.07	0.44	
Zr/TiO_2	**0.88**	**-0.71**	**-0.52**	**-0.83**	**-0.56**	**-0.75**	0.21	**0.78**	-0.34	0.03	**0.78**	-0.24	0.38	-0.05	0.06	**0.77**	-0.11	0.38	**0.79**

B. Altered rocks with molar K/(K + Na + 2Ca) less than 0.50

n = 71	SiO_2	TiO_2	Al_2O_3	Fe_2O_3	MgO	CaO	Na_2O	K_2O	Cu	As	Rb	Sr	Zr	Ag	Sb	Ba	Hg	Tl	K#
TiO_2	**-0.78**																		
Al_2O_3	**-0.73**	**0.83**																	
Fe_2O_3	**-0.73**	**0.85**	**0.70**																
MgO	**-0.68**	**0.56**	**0.59**	**0.67**															
CaO	**-0.51**	0.08	-0.02	0.00	0.16														
Na_2O	0.09	-0.15	-0.14	-0.11	-0.31	-0.07													
K_2O	0.07	-0.09	-0.13	-0.19	-0.34	-0.13	-0.29												
Cu	-0.48	**0.57**	0.36	**0.57**	0.43	0.08	0.06	0.05											
As	-0.03	0.08	0.19	0.08	-0.11	-0.16	-0.21	0.21	-0.01										
Rb	-0.05	0.07	0.02	-0.03	-0.20	-0.12	-0.44	**0.91**	0.07	0.31									
Sr	0.06	-0.11	-0.04	-0.14	-0.22	0.02	**0.71**	-0.25	0.11	-0.04	-0.38								
Zr	-0.01	0.16	0.41	0.06	-0.04	-0.31	0.00	0.05	-0.20	0.19	0.14	-0.05							
Ag	-0.14	0.21	0.05	0.28	0.19	-0.11	-0.24	0.30	0.27	0.19	0.29	-0.17	-0.26						
Sb	0.23	-0.07	-0.04	-0.13	-0.17	-0.27	-0.30	0.27	-0.19	0.44	0.24	-0.15	0.00	0.25					
Ba	0.43	-0.48	-0.39	**-0.56**	-0.46	-0.09	0.20	0.30	-0.26	-0.17	0.09	0.29	0.18	-0.20	0.05				
Hg	0.31	-0.22	-0.12	-0.31	-0.25	-0.17	-0.08	0.19	-0.15	0.24	0.06	0.04	0.03	0.21	**0.66**	0.29			
Tl	-0.21	0.24	0.15	0.15	0.00	-0.13	-0.39	**0.82**	0.21	0.33	**0.85**	-0.28	-0.01	0.47	0.27	0.01	0.17		
K#	0.24	0.02	0.11	-0.02	-0.13	**-0.67**	-0.42	**0.69**	-0.02	0.28	**0.69**	-0.42	0.28	0.30	0.37	0.09	0.17	**0.64**	
Zr/TiO_2	**0.67**	**-0.74**	-0.46	**-0.69**	**-0.53**	-0.27	0.17	0.11	**-0.59**	0.02	0.02	0.07	**0.51**	-0.33	0.04	**0.54**	0.26	-0.25	0.14

C. Altered rocks with molar K/(K + Na + 2Ca) equal to or greater than 0.50

n = 57	SiO_2	TiO_2	Al_2O_3	Fe_2O_3	MgO	CaO	Na_2O	K_2O	Cu	As	Rb	Sr	Zr	Ag	Sb	Ba	Hg	Tl	K#
TiO_2	**-0.76**																		
Al_2O_3	**-0.66**	**0.73**																	
Fe_2O_3	**-0.68**	**0.53**	0.20																
MgO	**-0.59**	0.44	0.15	**0.67**															
CaO	-0.48	0.26	0.28	0.33	0.26														
Na_2O	-0.42	0.20	0.24	0.19	0.40	0.20													
K_2O	0.10	-0.12	-0.23	-0.32	-0.39	-0.30	-0.14												
Cu	-0.26	0.26	0.24	0.27	0.07	0.17	0.00	-0.10											
As	0.42	-0.34	-0.39	-0.16	-0.46	-0.21	-0.16	0.24	-0.06										
Rb	0.01	-0.05	-0.14	-0.27	-0.35	-0.17	-0.12	**0.93**	0.00	0.18									
Sr	-0.14	-0.02	0.14	-0.27	-0.21	-0.07	0.42	**0.52**	-0.07	0.29	0.44								
Zr	-0.33	0.26	**0.60**	-0.09	0.10	0.20	0.22	-0.14	-0.07	-0.39	-0.05	0.06							
Ag	0.17	-0.03	-0.31	0.02	-0.18	-0.24	-0.22	0.30	0.10	0.33	0.27	-0.05	-0.31						
Sb	0.39	-0.31	-0.32	-0.10	-0.44	-0.06	-0.17	0.02	-0.07	**0.65**	0.01	0.08	-0.31	0.14					
Ba	-0.04	-0.07	0.05	-0.34	-0.23	-0.09	0.02	**0.61**	-0.07	0.08	**0.56**	**0.58**	0.10	-0.08	-0.06				
Hg	0.21	-0.21	-0.16	-0.21	-0.27	0.15	0.04	0.11	-0.09	0.31	0.10	0.26	-0.13	0.32	**0.58**	0.12			
Tl	0.27	-0.21	-0.30	-0.38	**-0.50**	-0.27	-0.18	**0.85**	-0.10	0.39	**0.80**	0.40	-0.26	0.42	0.38	0.45	0.45		
K#	**0.56**	-0.30	-0.33	-0.43	-0.48	**-0.86**	**-0.51**	**0.53**	-0.15	0.32	0.40	0.05	-0.25	0.34	0.11	0.19	-0.06	0.48	
Zr/TiO_2	**0.60**	**-0.76**	-0.31	**-0.53**	-0.38	-0.16	-0.06	-0.15	-0.24	0.15	-0.17	-0.04	0.21	-0.19	0.14	-0.08	0.02	-0.06	0.15

Notes: A. Unaltered Coromandel Group rocks (*n* = 98); B. Waitekauri area altered rocks with *M* K/(K + Na + 2Ca) < 1/2 (*n* = 71); C. Waitekauri area altered rocks with *M* K/(K + Na + 2Ca) ≥1/2 (*n* = 57); correlation coefficients equal to or greater than 0.50 or –0.50 are printed in bold

to 2.1 for andesite, and 1.8 or higher for dacites (Fig. 3C). There are no consistent differences in the value of Zr/TiO_2 at a given SiO_2 concentration between unaltered rocks of different Coromandel Group formations, which means the relationship between SiO_2 concentration and Zr/TiO_2 values is the same in all Coromandel Group rocks, even though they erupted over the course of 15.5 m.y. Therefore, the value of Zr/TiO_2 is a proxy for SiO_2 concentration in unaltered Coromandel Group rocks. Consequently, the Zr/TiO_2 value in altered Coromandel Group rocks can be used to estimate their initial igneous composition.

Estimation of Initial Rock Composition

Table 2A lists correlation coefficients for 18 elements and oxides with Zr/TiO_2 values in unaltered Coromandel Group rocks. Silica, TiO_2, K_2O, CaO, Fe_2O_3, Rb, and Ba concentrations correlate with Zr/TiO_2 with absolute coefficients greater than 0.7 and can therefore be estimated with some measure of precision based on a rock's Zr/TiO_2 value. Linear regression line equations for these elements versus Zr/TiO_2 can then be used to back-calculate unaltered-rock compositions (Table 3A). This approach is conceptually equivalent to the approach of MacLean (1990). In a Zr versus TiO_2 diagram, the method of MacLean (1990) relies on determining the intersection of a line through the origin with slope equal to a particular rock's Zr/TiO_2 ratio and a line that defines the covariation of Zr and TiO_2. The Zr or TiO_2 concentration at the intersection point can then be used to estimate protolith composition. A key difference with our approach is that we rely directly on the ratio Zr/TiO_2, rather than the absolute abundances of Zr or TiO_2, to infer protolith composition. As demonstrated in Figure 3 and Table 2A, the correlation between Zr/TiO_2 and SiO_2 (r = 0.88) is considerably stronger than that between SiO_2 and Zr (r = 0.24) or TiO_2 (r = –0.69) individually.

The amount of mass transferred for each element (ΔX) can then be calculated using the mass-balance equation of Gresens (1967). Although Gresens' (1967) formula required density data in addition to a chemical analysis, density data ultimately cancel out, and the formula was rewritten based solely on chemical data in the following form by Warren et al. (2007):

$$\Delta X = [(X^{Ai}/X^{Bi}) \times X^{B}] - X^{A}, \quad (1)$$

where X^A and X^B are the concentrations of an element in fresh and equivalent altered rock, respectively, and X^{Ai}/X^{Bi} is the ratio of the concentrations of an immobile constituent in unaltered and equivalent altered rock. Here we report results in g/100g (%) for major elements and in g/t (ppm) for trace elements. We use TiO_2 as the immobile element to calculate $X^{Ai}/X^{Bi}/X^{Ai}$, in this case, is the calculated TiO_2 concentration in the protolith, based on values of Zr/TiO_2 in the altered rock and using the equation in Table 3, whereas X^{Bi} is the measured concentration in the altered rock. TiO_2 has the advantage over Zr in that its concentration in protoliths correlates more strongly with Zr/TiO_2 values (Table 2A).

Effect of metasomatic TiO_2 loss

Some intensely altered rocks in our data set have experienced TiO_2 loss and consequently have anomalously large Zr/TiO_2 ratios. On this basis we have excluded eight altered rocks with Zr/TiO_2 values of 3 and greater from inclusion in the mass-balance approach. Some minor, cryptic loss of TiO_2 may have occurred in other altered rock samples and this would potentially have two effects (1) loss of TiO_2 raises the values of Zr/TiO_2, which leads to greater estimates for K_2O, Rb, Ba, Na_2O, and SiO_2 protolith concentrations, and lesser estimates for protolith concentrations of CaO, Fe_2O_3, MgO, and TiO_2 itself; and (2) loss of TiO_2 raises the values of X^{Ai}/X^{Bi}, leading to the apparent addition of mass to a rock. We modeled the result of these competing effects on calculated K_2O mass change for four different hypothetical altered rock compositions (Fig. 4). At a Zr/TiO_2 ratio of 1, typical of basaltic

TABLE 3. Linear Regression Equations Relating Element Concentrations to Zr/TiO_2 in Unaltered Coromandel Group Rocks

A			r	Avg. mass change	2σ
SiO_2	= 8.19X	+ 46.83	0.88	1.0 g/100g	16.8
K_2O	= 1.03X	– 0.16	0.77	0.0 g/100g	0.6
CaO	= – 2.71X	+ 11.07	–0.75	0.1 g/100g	2.7
Fe_2O_3	= – 2.89X	+ 11.52	–0.82	0.1 g/100g	1.8
Rb	= 43.09X	– 18.01	0.77	0.5 g/t	23.5
Ba	= 187.67X	– 19.67	0.77	3.6 g/t	113.5
TiO_2	= – 0.35X	+ 1.33	–0.71	N/A	N/A
B. Na_2O mass change			r	Avg. mass change	2σ
Waipupu Formation	= 1.14X	+ 0.75	0.90	0.5 g/100g	1.0
Whiritoa Andesite Formation	= 1.18X	+ 0.74	0.86	0.5 g/100g	1.0
C. MgO mass change			r	Avg. mass change	2σ
Waipupu Formation	= – 3.37X	+ 9.60	–0.86	–1.1 g/100g	2.9
Whiritoa Andesite Formation	= – 4.39X	+ 11.87	–0.87	–0.5 g/100g	2.7

X = $100Zr/TiO_2$

Notes: A. Equations based on the whole Coromandel Group data set (n = 98); B-C. Equations for Na_2O (B) and MgO (C) based on sample sets for Waipupu Formation (n = 10) and Whiritoa Andesite Formation (n = 7); the value r represents the correlation coefficient; "Avg. mass change" represents the average mass change in unaltered Coromandel Group rocks with double standard deviation 2σ

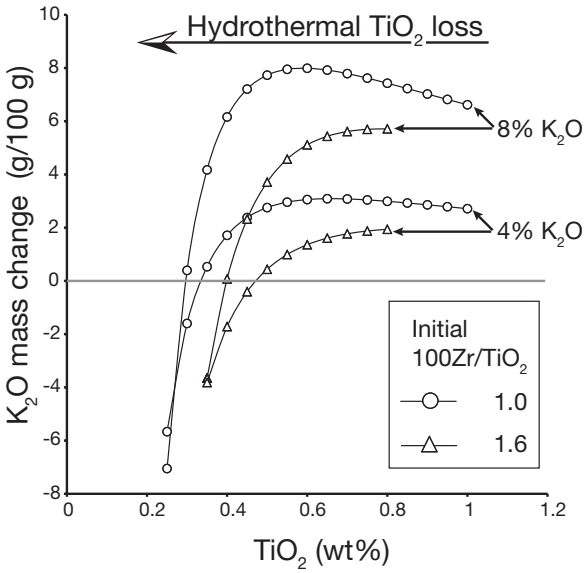

FIG. 4. Modeled outcomes of a K_2O mass-balance calculation for hypothetical altered rocks at increasing levels of TiO_2 loss, for two different measured K_2O concentrations and two different initial Zr/TiO_2 values. All altered rocks in this study have Zr/TiO_2 >1.

andesite, a loss of TiO_2 initially leads to a small apparent K_2O gain, and then to apparent K_2O loss as values of Zr/TiO_2 become very large. At a Zr/TiO_2 ratio of 1.6, typical for andesite, any loss of TiO_2 leads to an immediate decrease in estimated K_2O gain. We conclude that metasomatic TiO_2 loss will attenuate real K_2O gains for most rocks in this study, which are andesitic or dacitic in composition, and therefore this approach is robust because K_2O gains are not overestimated in rocks that have lost some TiO_2. The same trends apply for other element and oxide gains or losses.

Apparent mass change due to natural variation

Because concentrations do not correlate perfectly with Zr/TiO_2 values, apparent mass change can occur even in rocks that have not been altered. To assess the magnitude of this error, we used the equations in Table 3A and equation 1 to estimate mass change in the unaltered Coromandel Group rocks on which the equations are based. We use twice the standard deviation (2σ) of the apparent mass change in unaltered Coromandel Group rocks as a cut-off value to determine whether an altered rock shows significant mass change for an element: a significant loss or gain is where the mass change exceeds the 2σ value. Some elements may be initially lost and then gained during later alteration. The mass-balance calculation only yields the difference between the measured and initial amounts of mass; therefore, all gains and losses reported here are net gains and losses.

Sodium and magnesium concentrations in individual formations

Although Na_2O and MgO concentrations do not reliably correlate with SiO_2 in the Coromandel Group data set as a whole, they do in the Whiritoa Andesite (n = 7) and the Waipupu Formation (n = 10), which crop out widely in the southern Hauraki goldfield (Table 3). The linear regression equations for Na_2O and MgO versus Zr/TiO_2 value are very similar in both formations (Table 3B). However, using these equations to calculate mass change in all Coromandel Group rocks shows a considerable bias of at least –0.5 g/100 g for MgO and 0.5 g/100 g for Na_2O, with large 2σ errors of 1 g/100 g for Na_2O and ca. 2.8 g/100 g for MgO. Therefore, the Na_2O and MgO regression equations are of limited use for most Coromandel Group rocks. However, in this study we use, with caution, the equations derived for the Waipupu Formation, because altered rocks of this formation occur in much of the Waitekauri area.

Geochemistry of Altered Rocks

The gain of K and the loss of Na and Ca account for much of the mass transferred in shallow hydrothermal systems (Giggenbach, 1984, 1988). We evaluate K metasomatism in a diagram that plots molar (*M*) K/Al against *M* (K + Na + 2Ca)/Al (Fig. 5; Madeisky, 1996). In Figure 5, the slope of a line through the origin corresponds to the *M* ratio K/(K + Na + 2Ca) and ranges between 0 and 1. Increasing *M* K/(K + Na + 2Ca) in altered rocks indicates Ca and/or Na loss relative to K. A rock that has lost all Na + Ca has a *M* K/(K + Na + 2Ca) value of 1. Unaltered Coromandel Group rocks plot to the right of and around the plagioclase-adularia tie line, at K/Al values less than 0.25. Basaltic andesites have the greatest *M* (K + Na + 2Ca)/Al values, which are progressively lower in andesites and dacites.

Major element trends in altered rocks

The altered rocks of the Waitekauri area form two arrays in Figure 5. The illite-plagioclase array trends between unaltered Coromandel Group rocks, which have a plagioclase-dominated composition, and the clay mineral, illite. This array reflects loss of Ca and Na, coupled with limited gain of K, which causes rocks to change from a plagioclase-dominant igneous composition to an illite-dominant altered composition. The second array, which we refer to as the illite-adularia array, comprises rocks with *M* K/(K + Na + 2Ca) values close to 1 that plot along the illite-adularia tie line. A rock's location along this array mainly reflects variable replacement of adularia by illite. Altered rocks that form the illite-plagioclase array have up to 5 percent K_2O (Fig. 6A), which is less than the ca. 7.6 percent K_2O in illite—there are no altered rocks consisting entirely of illite. Altered rocks that plot on the illite-adularia array have much greater K_2O concentrations that range up to 10.4 percent, less than the 16.9 percent K_2O in adularia.

Element behavior during metasomatism

We evaluate the behavior of individual elements with increasing metasomatism in the Waitekauri area by plotting raw concentration data against *M* K/(K + Na + 2Ca) values (Fig. 6). K_2O and Rb concentrations consistently increase with *M* K/(K + Na + 2Ca), as expected (Fig. 6A-B). Thallium (not shown) is the only other element that shows this, presumably because it substitutes for K in adularia and/or illite (Gemmell, 2007). Barium concentrations do not increase consistently with *M* K/(K + Na + 2Ca) values but are commonly greater in altered rocks than in unaltered Coromandel Group rocks (Fig. 6C). SiO_2 concentration is greatest in altered rocks with

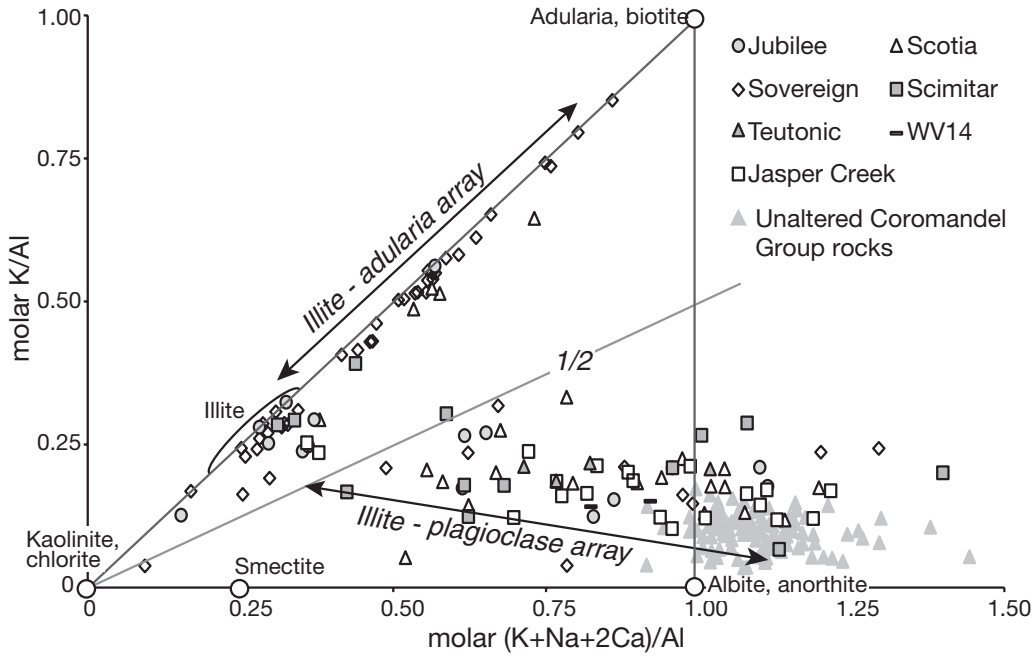

FIG. 5. Bivariate diagram of *M* (K + Na + 2Ca)/Al against *M* K/Al. After Madeisky (1996). Circles indicate the position of ideal mineral compositions. A line of *M* K/(K + Na + 2Ca) = 1/2 separates the altered rock sample sets used in the construction of Table 2B and C.

large *M* K/(K + Na + 2Ca) values, but some altered rocks with small *M* K/(K + Na + 2Ca) values have lower SiO_2 concentration than any unaltered Coromandel Group rocks (Fig. 6D). The concentrations of Al_2O_3, TiO_2, Zr, Th, and U, and the ratio Zr/TiO_2 do not change consistently with *M* K/(K + Na + 2Ca) values, therefore they were generally not significantly mobilized during metasomatism (Fig. 6E-J). Their concentrations show more scatter at greater *M* K/(K + Na + 2Ca), which likely reflects passive dilution or enrichment through the gain or loss of more mobile elements. However, Zr/TiO_2 values are anomalously large in some rocks with *M* K/(K + Na + 2Ca) values close to 1, which reflects metasomatic removal of TiO_2. As noted above, rocks with Zr/TiO_2 ratios greater than 3 are excluded from the mass-balance calculation. The concentrations of MgO and Fe_2O_3 vary little as *M* K/(K + Na + 2Ca) values increase up to 0.75 and show a gradual decrease in minimum and maximum concentrations at greater *M* K/(K + Na + 2Ca; Fig. 6K-L). We infer that Mg and Fe were relatively immobile during metasomatism, because they partition into chlorite and pyrite, respectively, but Fe and especially Mg concentrations can decrease significantly in the cores of hydrothermal alteration zones where chlorite may be less abundant. The concentrations of Na_2O, CaO, and Sr consistently decrease with increasing *M* K/(K + Na + 2Ca) values (Fig. 6M-O), which reflects their removal from altered rocks during K metasomatism.

Immobility of Th

The K_2O concentration in altered rocks, even at low *M* K/(K + Na + 2Ca) values, is typically greater than in unaltered rocks (Fig. 6A). As noted above, Th is relatively immobile during K metasomatism. The implication for geophysical exploration using radiometric K/Th data (e.g., Morrell et al., 2011) is that even mild K metasomatism will increase the K/Th value of the altered rocks. The K/Th ratio in unaltered Coromandel Group andesites and dacites ranges between 1,500 and 5,000, and unaltered basalts and rhyolites from the Hauraki goldfield have similar K/Th ratios (Fig. 7). In contrast, K/Th values in Waitekauri area altered rocks range up to 35,000; therefore any volcanic rocks in the Hauraki goldfield with K/Th values greater than 5,000 must have experienced K metasomatism.

Geochemical Zonation in the Waitekauri Area

We use two plots to illustrate spatial trends in the geochemistry of altered rocks in the Waitekauri area: diagrams that plot mass-change values versus the host rock's easting coordinates (Fig. 8A-H) and mass-change values for individual rock samples, projected onto three sections through the Waitekauri prospect (Fig. 9). We do not plot rock samples from the Teutonic prospect that are hosted in the Mangakara Dacite because of their unusually large Zr/TiO_2 values, although these rocks show only low-rank alteration as indicated by the presence of smectite and vein zeolites (Simpson and Mauk, 2011). In Figure 8, easting coordinates, in meters, are in reference to the New Zealand Map Grid. A dark gray line indicates zero mass change in each diagram and gray shading indicates the 2σ range as calculated in Table 3. Altered rocks that plot within this range have not experienced significant mass change for a given element. At any given point along the section, there are at least some rocks that have not experienced significant mass change. This underscores the necessity of acquiring a sufficiently large data base to ensure that geochemical trends are well represented. In the following discussion, we focus on maximum mass gains and losses, because for some elements and oxides these change laterally across

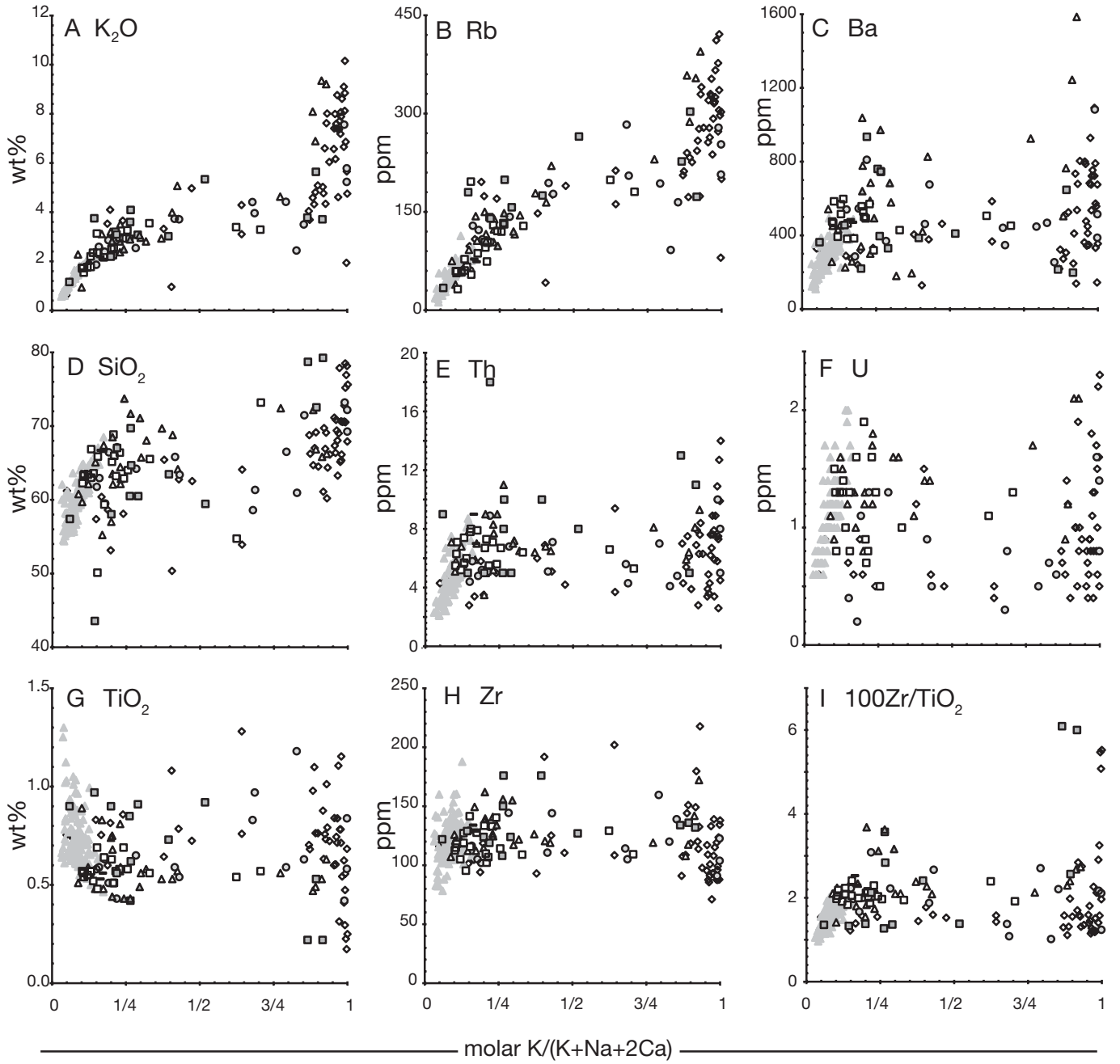

FIG. 6. Geochemical parameters plotted against *M* K/(K + Na + 2Ca). A-H. Major and trace element concentrations. I. Zr/TiO_2. Key in all diagrams as in Figure 5. J-O. Major and trace element concentrations plotted against *M* K/(K + Na + 2Ca). Key in all diagrams as in Figure 5.

the width of the Waitekauri area (e.g., K_2O, Fig. 8A; CaO, Fig. 8E). In addition, a dotted line indicates the moving average value calculated over each datapoint and the four points to either side.

For reference, we also plot values of Zr/TiO_2 against easting (Figs. 8I, 9A). Rocks from Sovereign, parts of Jubilee, and the western part of Scimitar have Zr/TiO_2 values mostly between 1 and 1.6, whereas rocks from eastern Scimitar, Scotia, Teutonic, and Jasper Creek have Zr/TiO_2 values around 2. This indicates that host rocks are more differentiated in the eastern deposits and prospects, consistent with the distribution of the Waitekauri Dacite and the andesitic Waipupu Formation (Fig. 1C).

Potassium and rubidium

Rubidium and K_2O correlate strongly in altered and unaltered Coromandel Group rocks (Table 2) and show identical spatial trends in maximum mass change (Fig. 8A-B). Maximum K_2O gains increase in a westward direction: from 2/100 g in rocks at Jasper Creek, to 7/100 g at Scotia, to 8/ 100 g at Jubilee, to 12.5/100g at Sovereign. Average gains also increase westward to a maximum of 5/100g at Sovereign. Maximum concentrations

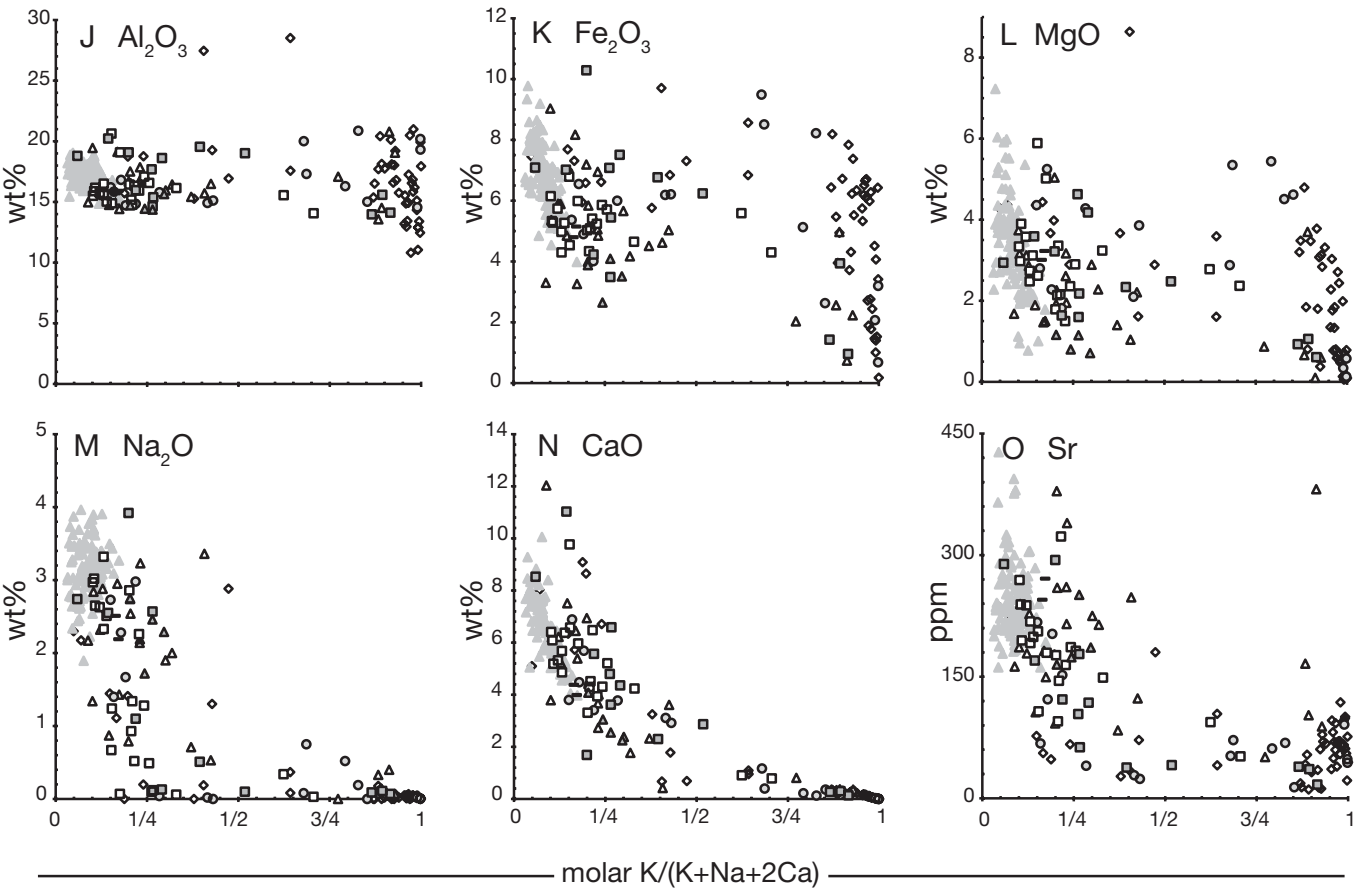

FIG. 6. *(Cont.)*

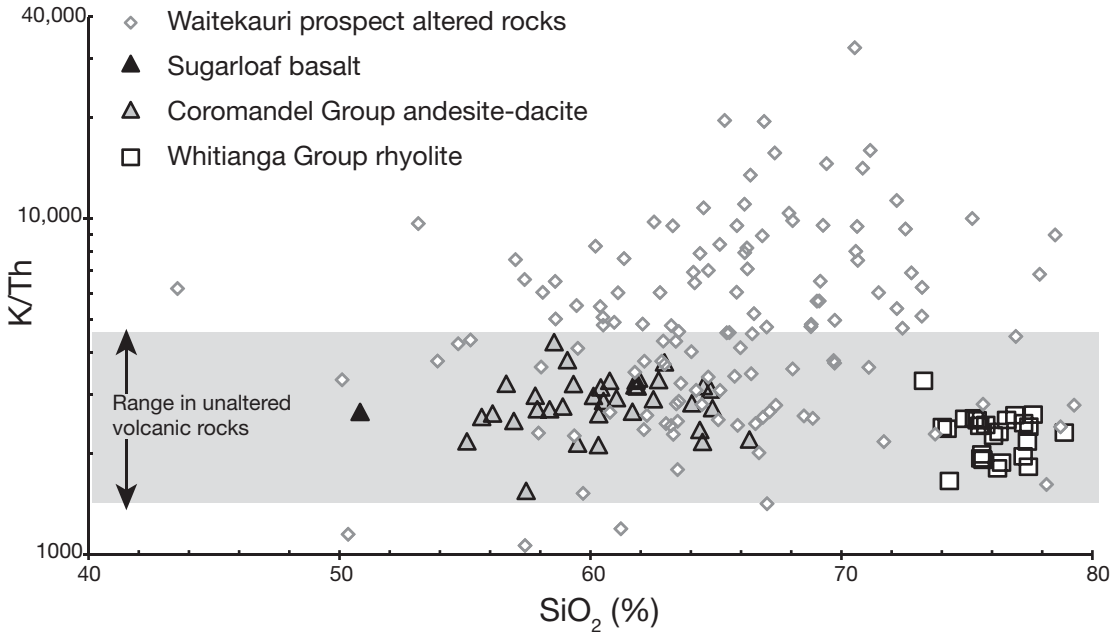

FIG. 7. Bivariate diagram of K/Th plotted against SiO_2. Sugarloaf basalt, Coromandel Group andesites and dacites, and Whitianga Group rhyolites represent unaltered arc volcanic rocks and represent the known range in volcanic rock composition in the Coromandel volcanic zone. Altered rocks are from the Waitekauri area.

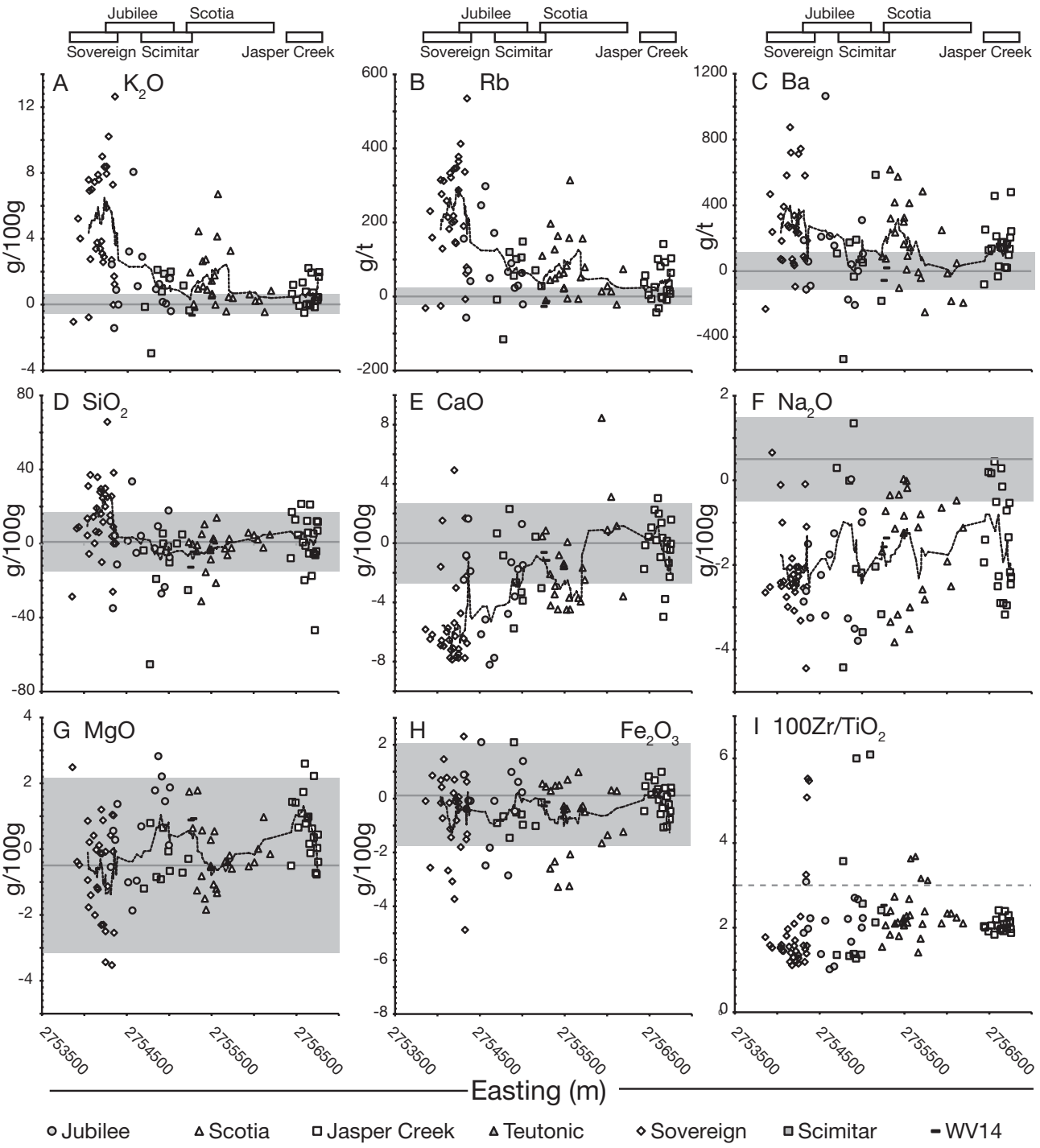

FIG. 8. A-H. Mass change in g/100 g against samples' easting coordinates in meters in reference to the New Zealand Map Grid. Dark gray lines indicate zero mass change, gray shading indicates the 2σ range of the apparent mass change in unaltered Coromandel Group rocks (Table 3). The bias and 2σ values for Na_2O and MgO are based on the application of the Waipupu Formation regression equations. Black dotted line indicates the average value calculated over each data point and the four data points to either side. I. Zr/TiO_2 plotted against samples' easting coordinates in meters in reference to the New Zealand Map Grid. Gray dashed line indicates the maximum Zr/TiO_2 for inclusion in the mass-balance calculation. Key in all diagrams as in Figure 5. J-O. Trace element concentrations in ppm plotted against samples' easting coordinates in meters in reference to the New Zealand Map Grid. Dark gray lines indicate the average concentration, gray shaded areas indicate the 2σ range in unaltered Coromandel Group rocks. Black dotted line indicates the average value calculated over each data point and the four data points to either side. P-R. Rb/Sr, *M* K/Al, and *M* K/(K + Na + 2Ca) values plotted against samples' easting coordinates in meters in reference to the New Zealand Map Grid. Dark gray lines and gray shading indicate the average values and 2σ range in unaltered Coromandel Group rocks. Black dotted line indicates the average value calculated over each data point and the four data points to either side. In P and Q the average is calculated as the median. Key in all diagrams as in Figure 5.

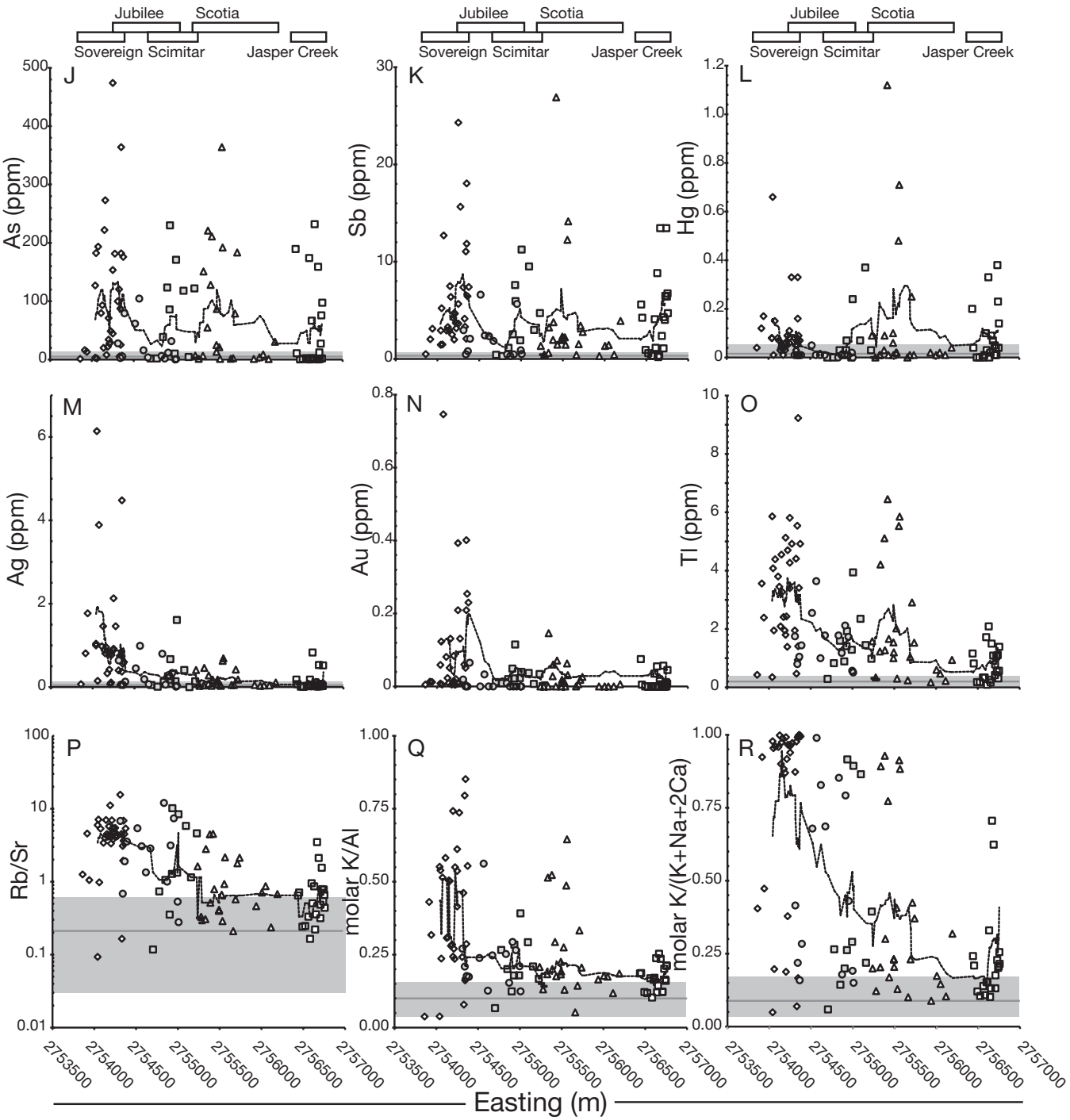

FIG. 8. *(Cont.)*

of K_2O in the altered host rocks at the Scotia and Sovereign deposits are comparable at 9.4 and 10.2 percent, respectively, but the maximum gains for K_2O at these deposits are 7/100 g and 12.5/100g, respectively, showing that rocks at Sovereign have experienced much greater K metasomatism (Fig. 10).

The westward increase in maximum and average K_2O gain correlates with the increasing proportion of adularia (Fig. 9K; Simpson and Mauk, 2011) and with the increasing dominance of illite over smectite (Fig. 9L). Illite is the dominant K-bearing mineral at Scimitar, and it occurs with adularia in most of the sampled rocks at Sovereign, Jubilee, and Scotia (Simpson and Mauk, 2011). Adularia occurs in some shallow rocks at Jasper Creek, at Scotia in a shallow carapace, locally at Jubilee, and extensively at Sovereign. At the Sovereign, Jubilee, and Scotia deposits, the presence of adularia correlates with substantial K_2O gain; as indicated above, the greatest K metasomatism is at the Sovereign deposit, which has the most widespread adularia alteration (Fig. 9K).

FIG. 9. Geochemical parameters for each sample, projected onto the sections shown in Figure 1D. A. Zr/TiO_2. B. K_2O mass change. C. Ba mass change. D. SiO_2 mass change. E. CaO mass change. F. Na_2O mass change. G. As concentration. H. Sb concentration. I. Au concentration. J. Ag concentration. In sections (B)-(J) white indicates rocks with no significant gain or loss. K-N. Distribution of alteration minerals, after Simpson and Mauk (2011). Sections are located as shown in Figure 1C.

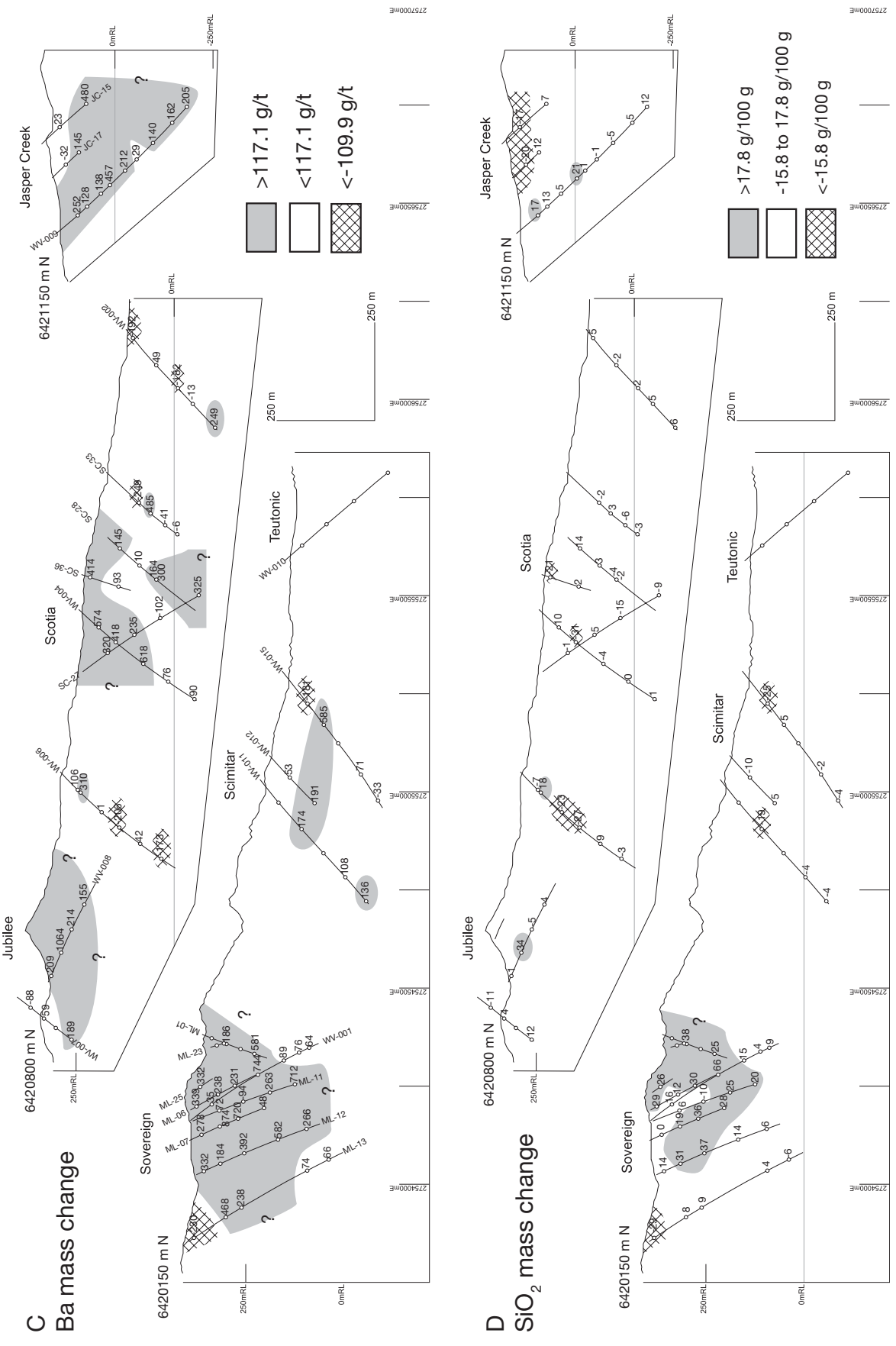
C
Ba mass change
D
SiO2 mass change
>117.1 g/t
<117.1 g/t
<-109.9 g/t
>17.8 g/100 g
-15.8 to 17.8 g/100 g
<-15.8 g/100 g
Jasper Creek
Jubilee
Scotia
Teutonic
Scimitar
Sovereign
6421150 m N
6420800 m N
6420150 m N
0mRL
250mRL
-250mRL
250 m
2757000mE
2756500mE
2756000mE
2755500mE
2755000mE
2754500mE
2754000mE

FIG. 9. *(Cont.)*

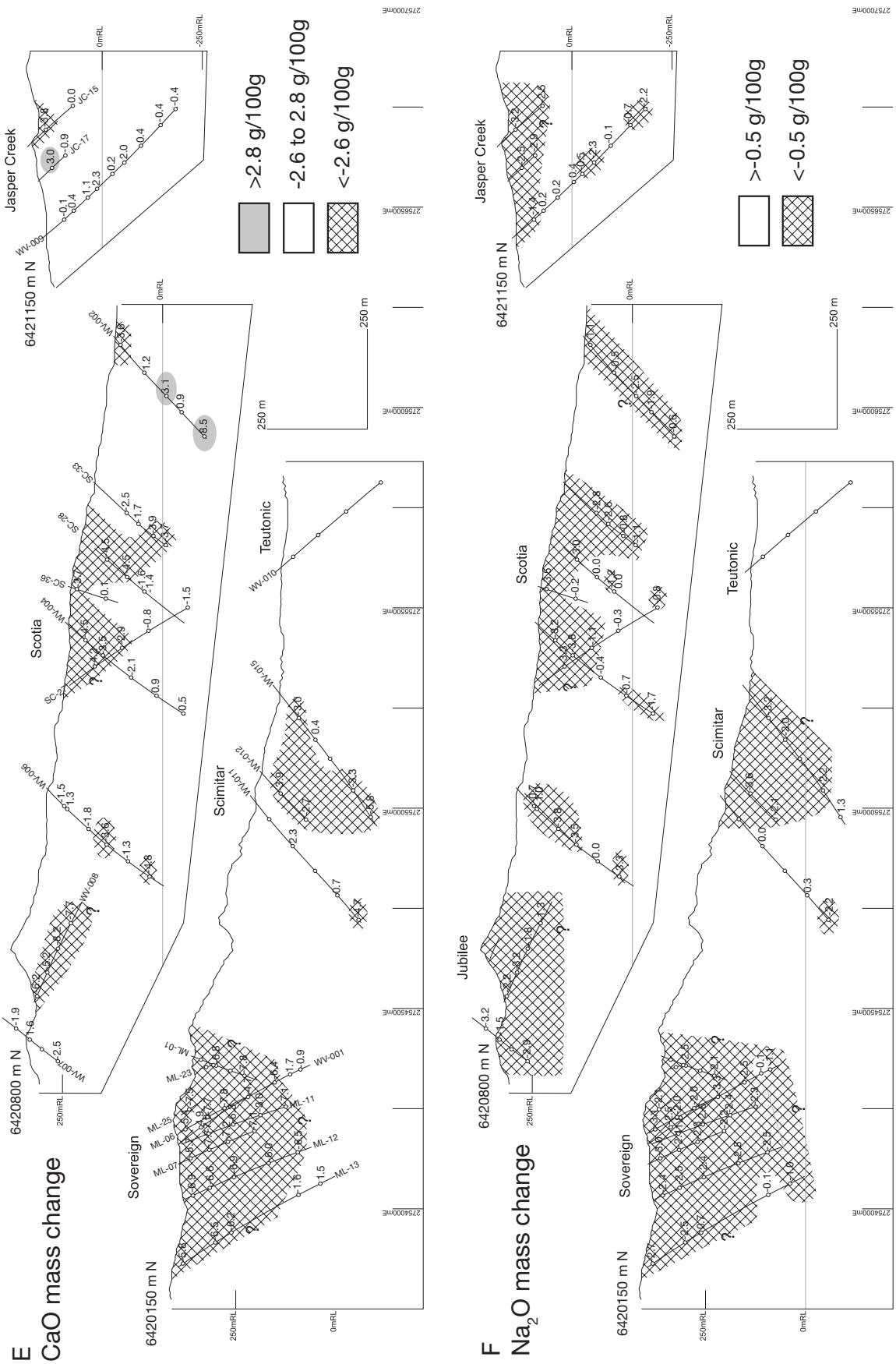
E
CaO mass change
F
Na_2O mass change
>2.8 g/100g
-2.6 to 2.8 g/100g
<-2.6 g/100g
>-0.5 g/100g
<-0.5 g/100g
Jasper Creek
Jubilee
Scotia
Teutonic
Scimitar
Sovereign
6421150 m N
6420800 m N
6420150 m N
0mRL
250mRL
-250mRL
250 m
2757000mE
2756500mE
2756000mE
2755500mE
2755000mE
2754500mE
2754000mE

FIG. 9. *(Cont.)*

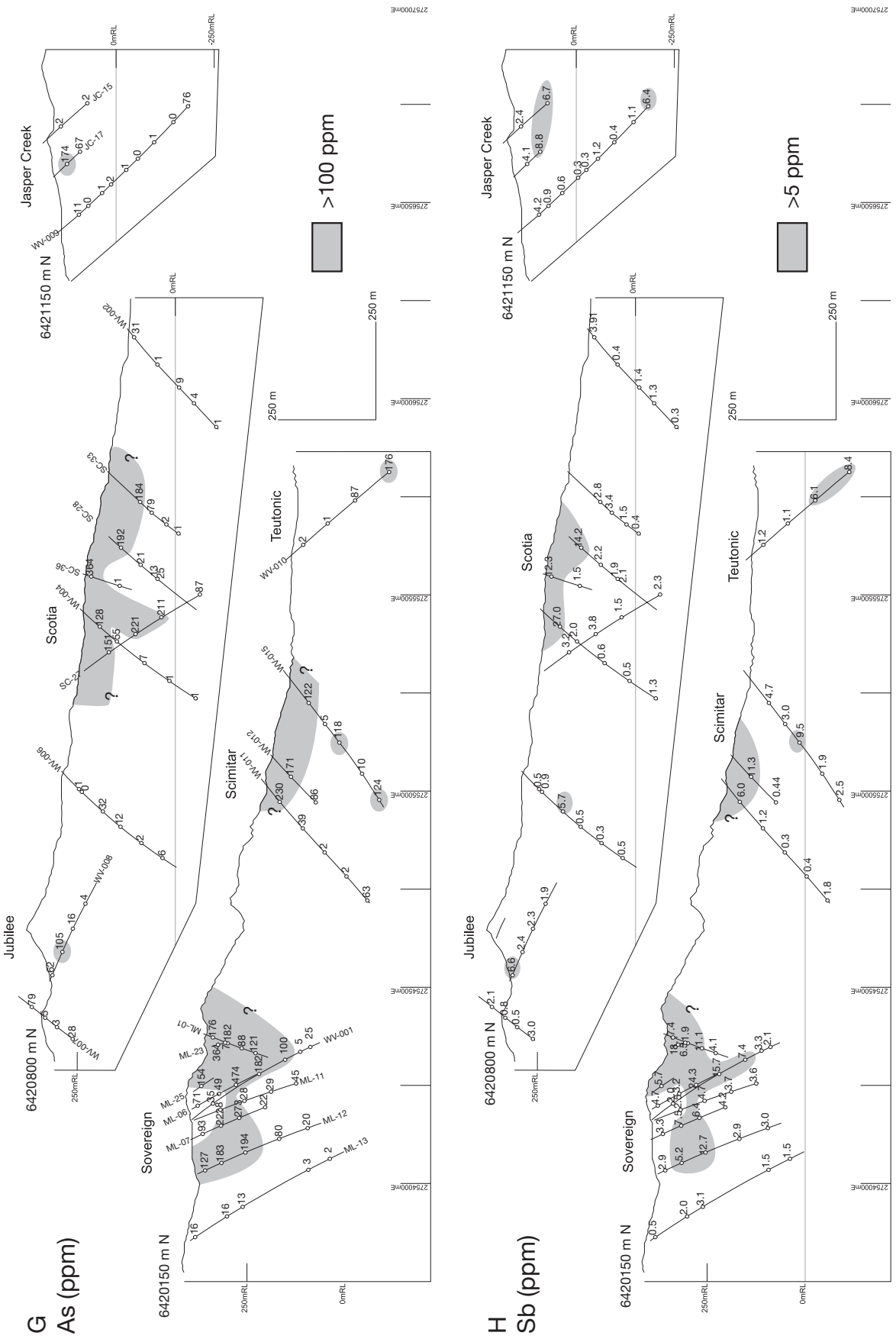
G
As (ppm)
H
Sb (ppm)
>100 ppm
>5 ppm
Jasper Creek
Jubilee
Scotia
Scimitar
Sovereign
Teutonic
6421150 m N
6420800 m N
6420150 m N
0mRL
250mRL
-250mRL
250 m
2757000mE
2756500mE
2756000mE
2755500mE
2755000mE
2754500mE
2754000mE

FIG. 9. *(Cont.)*

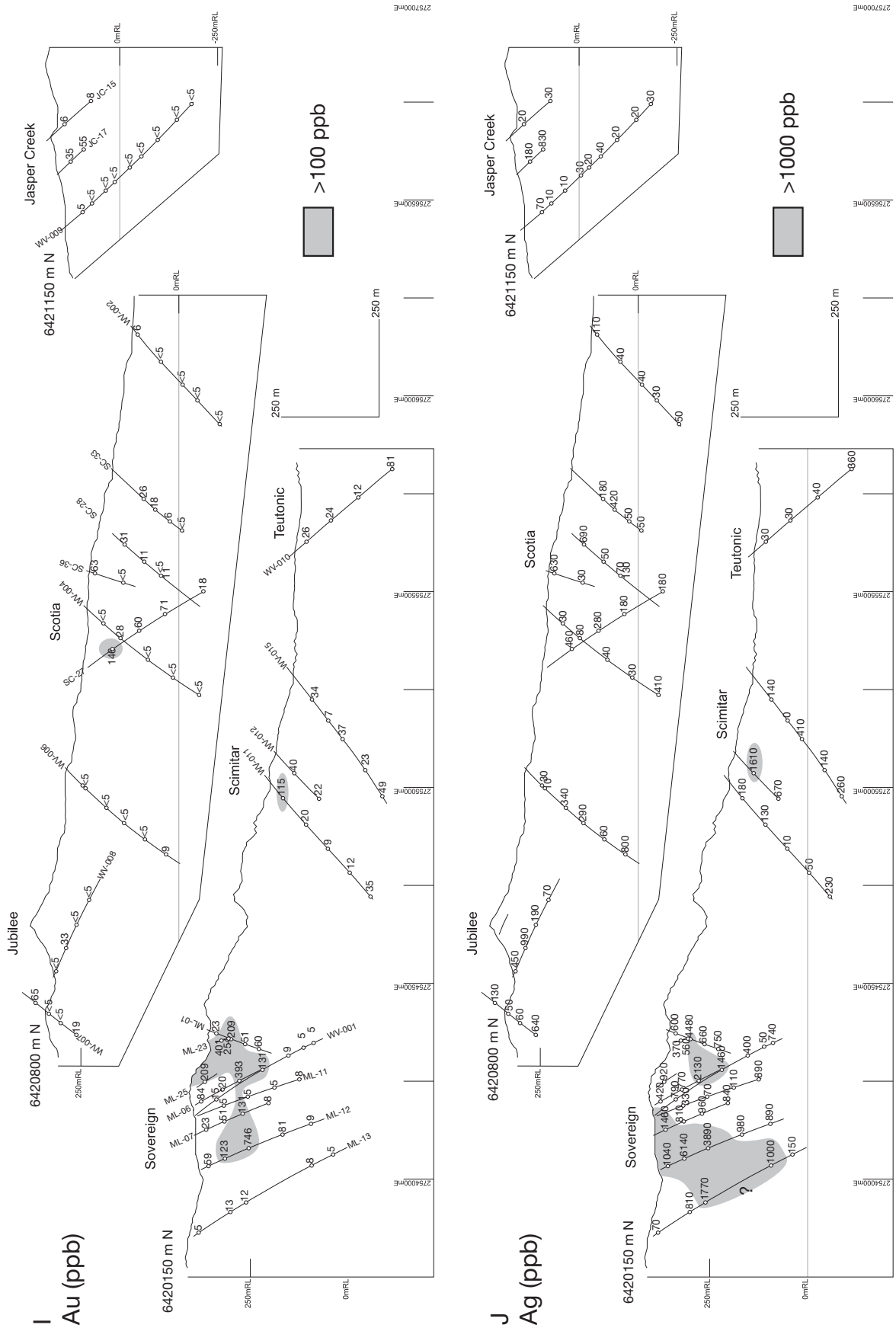
I
Au (ppb)
J
Ag (ppb)
Jubilee
Scotia
Scimitar
Teutonic
Sovereign
Jasper Creek
6421150 m N
6420800 m N
6420150 m N
>100 ppb
>1000 ppb
250 m
0mRL
250mRL
-250mRL
?

FIG. 9. *(Cont.)*

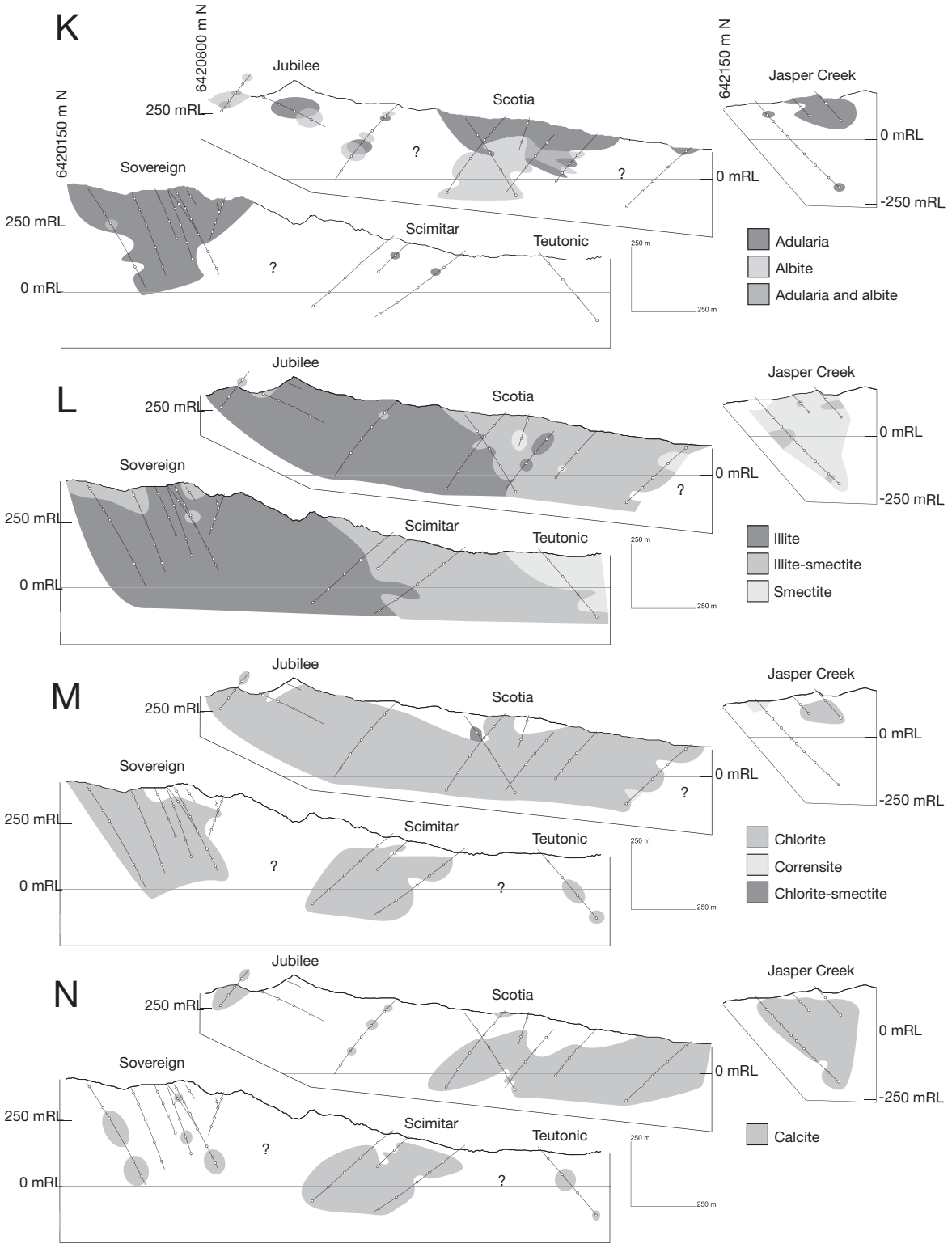

FIG. 9. *(Cont.)*

Barium

Barium concentration correlates with K_2O and Rb concentrations in unaltered Coromandel Group volcanic rocks but less strongly in altered rocks (Table 2); nevertheless maximum Ba gains show a relatively clear gradient across the Waitekauri area (Fig. 8C). Most samples at the Jasper Creek prospect show Ba gains of up to 200 g/t with two outliers up to 500 g/t. Maximum Ba gains at Scimitar and Scotia are approximately 600 and 900 g/t at the Sovereign deposit. Maximum Ba gains therefore parallel the regional

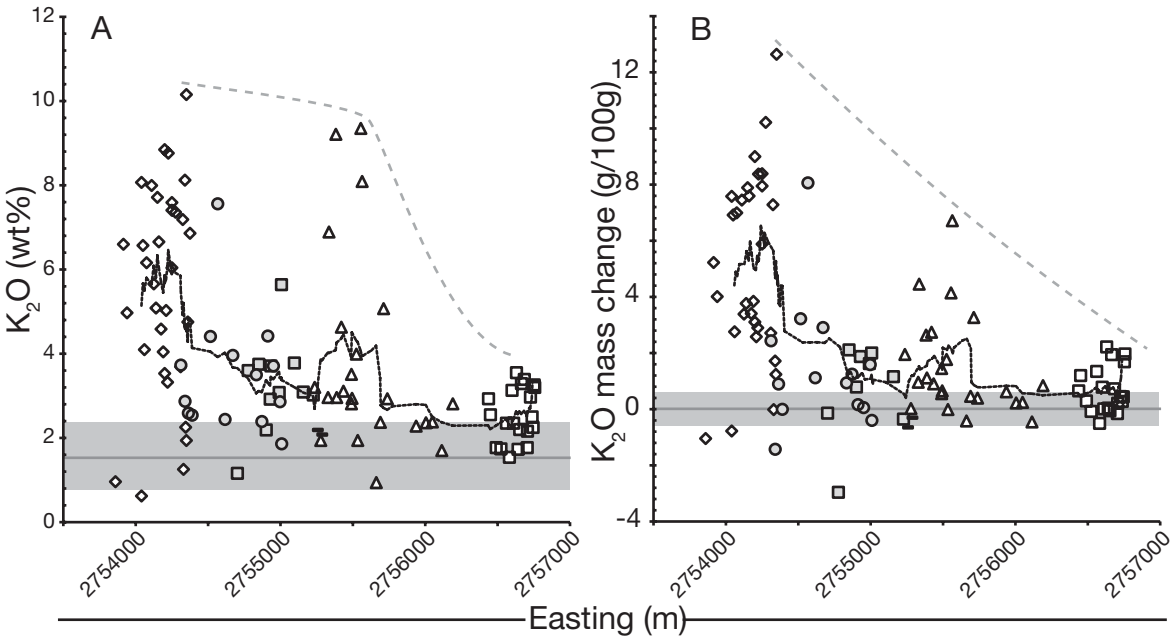

FIG. 10. A. Raw K_2O concentrations plotted against samples' easting coordinates in meters in reference to the New Zealand Map Grid. Dark gray line and gray shaded area indicate average and 2σ range in unaltered Coromandel Group rocks. B. K_2O mass change plotted against samples' easting coordinates in meters in reference to the New Zealand Map Grid. Dark gray line indicates zero mass change, gray shaded area indicates the 2σ range of the apparent mass change in unaltered Coromandel Group rocks (Table 3). Dotted lines indicate the average value calculated over each data point and the four data points to either side, and dashed lines indicate the maximum value trend. Key in both diagrams as in Figure 5.

trend in maximum and average K_2O and Rb gains, where the greatest Ba gains occur in adularia-rich rocks (Fig. 9C, K).

Silicon

Most altered rocks in the Waitekauri area show no significant SiO_2 loss or gain (Fig. 8D). Greater SiO_2 gains and losses mostly occur at shallow levels (Fig. 9D), corresponding to areas of greater K_2O gains in the upper levels of Scotia and Scimitar (Fig. 9B), and to the distribution of adularia and albite at Scotia (Fig. 9K). Silica gains are generally greatest in the most strongly altered rocks, which have the greatest concentration of hydrothermal quartz (Simpson and Mauk, 2011). Our sampling excluded all veins and veinlets in the host rocks; if these had been included, more samples would show SiO_2 gains. Maximum SiO_2 gains are greatest in rocks at the Sovereign deposit, whereas most host rocks from the Jasper Creek, Teutonic, and Scimitar prospects show no significant SiO_2 gain (Fig. 8D). A limited number of host-rock samples, from throughout the Waitekauri area, show significant SiO_2 losses. These rocks do not have a specific mineralogical composition that contrasts with other altered rocks, therefore their low SiO_2 content might reflect a high proportion of clay minerals and/or chlorite relative to feldspar and quartz.

Sodium and calcium

All deposits and prospects, except the peripheral Jasper Creek and Teutonic prospects, have some rocks with <0.2 percent CaO—it has almost entirely been removed by hydrothermal alteration. Maximum CaO loss is greatest in rocks at Sovereign and Jubilee, lower at Scimitar, and lower again at Scotia and Jasper Creek (Fig. 8E). However, this trend is an artefact of rock type: the andesitic host rocks at Sovereign, Jubilee, and western Scimitar had greater initial CaO concentrations and therefore could lose more CaO during alteration than the dacitic rocks at Scotia and Jasper Creek.

Maximum Na_2O losses exceed 3/100 g at each deposit and prospect (Fig. 8F), although as noted above, Na_2O protolith concentration estimates are probably inaccurate if host rocks are not part of the Waipupu Formation. Losses are generally greater in rocks at Scimitar and Scotia than in rocks at Sovereign. This reflects the greater initial Na_2O concentration in unaltered dacite relative to unaltered andesite, and therefore maximum Na_2O loss trends are an artefact of rock type.

All altered rocks that show Na_2O loss also show CaO loss, and areas of significant Na_2O loss extend farther than those of significant CaO loss at each deposit and prospect (Fig. 9E-F). Calcium gains occur in rocks containing calcite at Teutonic and eastern Scotia, but most rocks that contain calcite also show limited CaO loss (Fig. 9N). This reflects the typically late-stage nature of calcite precipitation (Simpson and Mauk, 2011), which occurred in rocks that had lost some or all CaO during main-stage alteration. Hydrothermal albite at the Scotia and Jubilee deposits typically occurs in altered rocks that show limited Na_2O loss (Fig. 9K).

Iron and magnesium

Chlorite is the principal alteration mineral that hosts Mg and Fe^{2+}; it is abundant in most rocks in the Waitekauri area (Fig. 9M). Pyrite is also ubiquitous, even in the most iron poor rocks, and indicates the addition of S to the altered rocks (Simpson and Mauk, 2011). The greatest Fe_2O_3 and MgO

losses occur in adularia-bearing rocks at the Sovereign and Jubilee deposits in the west (Fig. 8G-H). This trend partly reflects greater initial concentrations in the andesitic host rocks in the western deposits and partly the lower abundance of chlorite in intensely metasomatized rocks. Host rocks at the Jubilee deposit and the Jasper Creek prospect show preferential MgO gain instead of loss. There is no clear correlation between MgO gain and the presence or absence of any of the alteration minerals considered in this study.

Precious metal and pathfinder element concentrations

Although precious metals and pathfinder elements mainly occur in vein minerals, they also show a wide range in concentrations in altered rocks of the Waitekauri area. These elements occur in trace amounts in unaltered Coromandel Group rocks (Table 2A), and they can be enriched by two orders of magnitude in altered rocks (Table 1). Therefore, rather than calculating mass change, we simply use raw whole-rock concentrations to assess whether they reflect proximity to mineralization or regional or local gradients in alteration intensity.

The traditional epithermal pathfinder elements, As, Sb, and Hg, are anomalous in the altered rocks of the Waitekauri area, and they show similar distributions, but they do not show a clear gradient on the scale of this section (Fig. 8J-L). The greatest concentrations occur at the Sovereign and Scotia deposits but, except for four outliers, the maximum concentrations of As, Sb, and Hg are similar in altered rocks at Sovereign, Scimitar, Scotia, and Jasper Creek and are somewhat lower at the Jubilee deposit. Concentrations of pathfinder elements are highly variable on a local scale, changing by an order of magnitude or more over 100-m-scale distances (Fig. 9G-H). In contrast, the maximum concentrations of Au and Ag are similar in altered rocks at Jasper Creek, Scotia, Scimitar, and Jubilee but substantially greater at the Sovereign deposit (Fig. 9I-J) where they correlate with K and Si gains (Fig. 9B, D). At the Sovereign deposit, Au and Ag occur in silicified and fractured breccia zones and in narrow veins, in contrast to other areas where Au occurs in veins in lava flows, and it is possible that the elevated Au contents in Sovereign rocks relates to microbrecciation and/or silica flooding (Simpson and Mauk, 2011). Maximum Tl concentrations increase from Jasper Creek to Scotia to Sovereign, although, with the exception of one outlier, similar maximum concentrations occur at the Sovereign and Scotia deposits, with considerably lower maximum concentrations at Jubilee and Scimitar (Fig. 8O).

We conclude that precious metal concentrations closely correlate with quartz-adularia–rich rocks that surround Au deposits along the Waitekauri fault. Pathfinder element concentrations, in contrast, are anomalously high in specific alteration cells throughout the Waitekauri area, but their concentrations do not define a gradient from the central Waitekauri fault to the peripheral Jasper Creek prospect.

Other geochemical parameters

Apart from a mass-balance calculation, the intensity of K metasomatism can be expressed by geochemical parameters, including K/Sr, Rb/Sr, *M* K/Al, and *M* K/(K + Na + 2Ca) ratios (Madeisky, 1996; Mauk and Simpson, 2007; Warren et al., 2007). Average and maximum values for these parameters show clear westward trends in the Waitekauri area. K/Sr and Rb/Sr values have identical distributions (we only show Rb/Sr: Fig. 8P) with a marked increase in median value westward, although maximum values are similar at Sovereign, Jubilee, and Scimitar. Both median and maximum *M* K/Al values also increase westward and maximum values are distinctly greater at Sovereign than at Scotia (Fig. 8Q). Molar K/(K + Na + 2Ca) shows the most distinct increase in average value westward, directly comparable to the trends in maximum and average K_2O and Rb gain (Fig. 8R). It is striking that *M* K/(K + Na + 2Ca) correlates so closely with the distribution of adularia, given that illite and adularia both have *M* K/(K + Na + 2Ca) values of 1. This most likely reflects the more complete leaching of Na and Ca from, and the lack of late-stage calcite in, adularia-rich rocks.

Summary of alteration geochemical trends

The principal mass-change parameters that define a regional gradient toward Au-Ag deposits along the Waitekauri fault are maximum and average K_2O, SiO_2, Rb, and to a lesser extent Ba gains, which increase from east to west in the Waitekauri area along a 3-km-wide section (Fig. 8A-D). Mass gains for K_2O, SiO_2, Rb, and Ba are greatest in adularia-rich rocks at the Sovereign deposit. The increase in K metasomatism is obscured by variation in protolith composition, which leads to similar maximum K_2O concentrations in altered rocks of 10.2 percent at Sovereign and 9.4 percent at Scotia, although we note that average K_2O concentrations show a similar trend to K_2O gains (Fig. 10). Other major elements are lost during metasomatism or remain immobile. Elements that are lost can theoretically yield a vector toward the core of an alteration zone, however in the Waitekauri area such elements do not yield clear trends in maximum or average loss. Calcium and Na are commonly completely lost during alteration, therefore the trends in average and maximum CaO and Na_2O losses do not reflect the increasing alteration intensity and metasomatism toward the west but rather protolith heterogeneity: a greater initial concentration of mobile elements means that more mass can be lost (Fig. 8E-F). The maximum losses of MgO and Fe_2O_3 increase westward, but the average losses do not show a distinct trend (Fig. 8G-H), which reflects the relative stability under K metasomatism of chlorite and pyrite, the main alteration minerals that host Mg and Fe (Fig. 6K-L).

Several geochemical parameters that do not require a mass-balance calculation correlate with K_2O mass gain: maximum and average K/Sr, Rb/Sr, *M* K/Al, and particularly *M* K/(K + Na + 2Ca) values all increase from east to west in the Waitekauri area (Fig. 8P-R). In contrast, the maximum and average concentrations of the pathfinder elements As, Sb, and Hg are similar at Jasper Creek, Scotia, Jubilee, and Sovereign, and therefore pathfinder elements do not show distinct trends across the Waitekauri area. Taken together, we suggest that pathfinder elements can identify smaller cells of hydrothermal mineralization, which may or may not be economic. In contrast, K and Si mass gains, K/Sr, Rb/Sr, and *M* K/(K + Na + 2Ca) values suggest that the main locus of hydrothermal fluid flow was in the western deposits of the Waitekauri area, where it was focused by the Waitekauri fault (Simpson and Mauk, 2011; Grodzicki et al., unpub. data).

Discussion

Vectors toward orebodies

From an exploration point of view, metasomatism would ideally increase gradually toward the core of an alteration zone. This is unlikely in reality as faults, fractures, and heterogeneous host rock lithology and permeability constrain hydrothermal fluid flow on a range of scales in any setting (e.g., Cox et al., 2001; Person et al., 2008; Rosenberg et al., 2009). In the Waitekauri area, the overall westward trend in K and Si gains and K/(K + Na + 2Ca) values is superimposed on considerable local variation: strong vertical gradients in K_2O gain and CaO loss exist at Scotia and Jasper Creek and correlate with the presence of adularia in shallow rocks; K_2O gains at Sovereign are greatest in shallow rocks, even though adularia occurs to depth (Fig. 9B, E, K). The deposits and prospects of the Waitekauri area, which are defined by the altered rocks at the surface, are also separated by areas with less altered rocks (Fig. 9B; Morrell et al., 2011). This kind of variation is to be expected in an alteration zone developed in a complex volcanic stratigraphy comprising massive and autobrecciated lava flows, tuffs, and tuff breccias intruded by dikes and cut by normal faults (Brathwaite and Christie, 1996; Haworth and Briggs, 2006; Simpson and Mauk, 2011; Grodzicki et al., 2011). Nevertheless, clear regional trends exist in the Waitekauri area in maximum and average K and Si mass gains, Rb/Sr values, and *M* K/(K + Na + 2Ca) values. The geochemical trends persist across a 3-km-wide section, correlate with trends in fluid inclusion homogenization temperature, alteration mineralogy and radiometric K/Th data, and vector toward Au-Ag deposits hosted in adularia-rich rocks at the core of the alteration zone (Morrell et al., 2011; Simpson and Mauk, 2011).

The west-directed mass-change gradient reaches a maximum at the Sovereign deposit, and we speculate that this may either be the result of strong hydrothermal fluid upwelling along the Waitekauri fault and related faults or may reflect an ongoing gradient of increasing mass change to areas farther to the west and northwest. The area west of Sovereign has not been thoroughly explored because the postmineral Whakamoehau Andesite Formation at the surface covers the Waipupu Formation (Fig. 1B), which is the likely host of any orebodies there, and therefore exploration would have to take place through postmineral cover. Nonetheless, whole-rock geochemical data from the area west of Sovereign could determine whether K metasomatism is stronger or weaker on the western side of the Waitekauri fault and whether that area is prospective for mineralization.

Mass transfer in the Waitekauri-Maratoto area

The mass-balance calculations presented here, coupled with new data on the extent of altered rocks in the Waitekauri area (Morrell et al., 2011), provide the opportunity to estimate the total amount of mass transferred in the Waitekauri-Maratoto area. Airborne radiometric surveys reveal a ~24-km^2 area where K/Th is increased from unaltered volcanic values, within which occur anomalies of very high K/Th. The larger high K/Th zone overlaps with the magnetic quiet zone (Morrell et al., 2011). The very high K/Th anomalies occur along the Waitekauri fault and elsewhere in the Waitekauri-Maratoto area and collectively comprise 9.3 percent of the larger altered zone. The larger high K/Th zone reflects the overall extent of K metasomatism, whereas the localized, very high K/Th anomalies reflect intense, localized K metasomatism (cf. Fig. 6A). We assume here for simplicity that rocks with illite (including interstratified illite-smectite), but without adularia, cause the generally elevated K/Th values in the larger Waitekauri-Maratoto area, and that the very high K/Th anomalies within this larger area are associated with adularia-bearing rocks such as those at Sovereign. The illite-bearing rocks in the Waitekauri area on average gained K and lost Si, Na, Ca, Mg, and Fe. Assuming immobility of Al and Ti, and disregarding P, the total major element oxide mass transferred (i.e., gained as well as lost) in illitic alteration is ca. 11 percent of the rock mass. The adularia-bearing rocks at Sovereign on average gained K and Si, and lost Na, Ca, Mg, and Fe, with a total major element oxide mass transfer equal to 24 percent of the rock mass. K_2O accounts for 71 percent of the gained mass in altered rocks and SiO_2 for the remainder, where significant SiO_2 gains are confined to adularia-rich rocks that surround epithermal deposits along the Waitekauri fault.

If 9.3 percent of the 24-km^2 Waitekauri-Maratoto altered zone consists of very high K/Th, adularia-bearing rocks like those at Sovereign, and the rest consists of illite-bearing rocks, and if alteration extends downward 1 km with the same distribution of altered rock types, and if the average density of the altered rocks is 2.65 g/cm^3, then the total mass of rocks in the Waitekauri-Maratoto area is $6.4 \cdot 10^{10}$ t, and the total mass transferred is approximately $7.5 \cdot 10^9$ t, equal to 12 percent of the rock mass. However, the actual mass transferred is likely to be greater than this because the mass-balance calculation only returns a net mass-change estimate. Mass losses exceed mass gains in adularia-, as well as in illite-dominated altered rocks. We only analyzed veinless altered rocks; it is possible that some of the mass that was lost from altered rocks, especially Si and Ca, was redeposited as vein-filling minerals.

Relationship between geochemistry and alteration mineralogy

During hydrothermal alteration, host rocks in the Waitekauri area lost Na and Ca and gained K, producing end-member altered rocks with *M* K/(K + Na + 2Ca) values close to 1 (Fig. 5). Potassium is contained in illite and/or adularia. Illite (K mica) contains approximately 7.6 percent K_2O and adularia contains 16.9 percent K_2O. Therefore, 7.6 percent is the maximum K_2O concentration for altered rocks without adularia, whereas 16.9 percent is the theoretical maximum concentration of K_2O in altered rocks, as no other rock-forming alteration mineral in epithermal deposits has a greater K_2O content than adularia. All rocks in the Waitekauri area with more than 7.6 percent K_2O have *M* K/(K + Na + 2Ca) values close to 1 and therefore contain no significant Ca and Na. Coupled with the lack of data points outside the illite-plagioclase and illite-adularia arrays, this suggests that the adularia-bearing altered rocks in the illite-adularia array only formed from illite-dominated altered rocks (Fig. 5). This is consistent with the expected succession of mineral precipitation during the dissolution of increasing amounts of rock by a hydrothermal fluid (Giggenbach, 1984).

Petrographic relationships indicate that adularia, where present, is variably replaced by illite (Simpson and Mauk,

2011). This is plausibly the result of waning of the hydrothermal system. Alternatively, it is possible that some volcanic rocks were directly altered to an adularia-dominated composition, from which adularia-rich rocks were subsequently altered toward an illite-dominated composition. A possible corresponding set of dual reaction pathways has been inferred at the Broadlands-Ohaaki geothermal system in the central North Island. There, boiling of chloride-rich water in central upflow zones forms adularia and illite, whereas peripheral mixing of chloride-rich water with CO_2-rich water produces only illite as a K-bearing phase in host rocks (Simmons and Browne, 2000). However, in the *M* K/Al versus (K + Na + 2Ca)/Al diagram from the Waitekauri area, there is a gap with no samples that lies between unaltered rocks and adularia (Fig. 11A). If the adularia-bearing rocks in the illite-adularia array in the Waitekauri area are derived from adularia-dominated rocks, rather than illite-dominated rocks, the alteration reaction from plagioclase to adularia dominated must therefore have

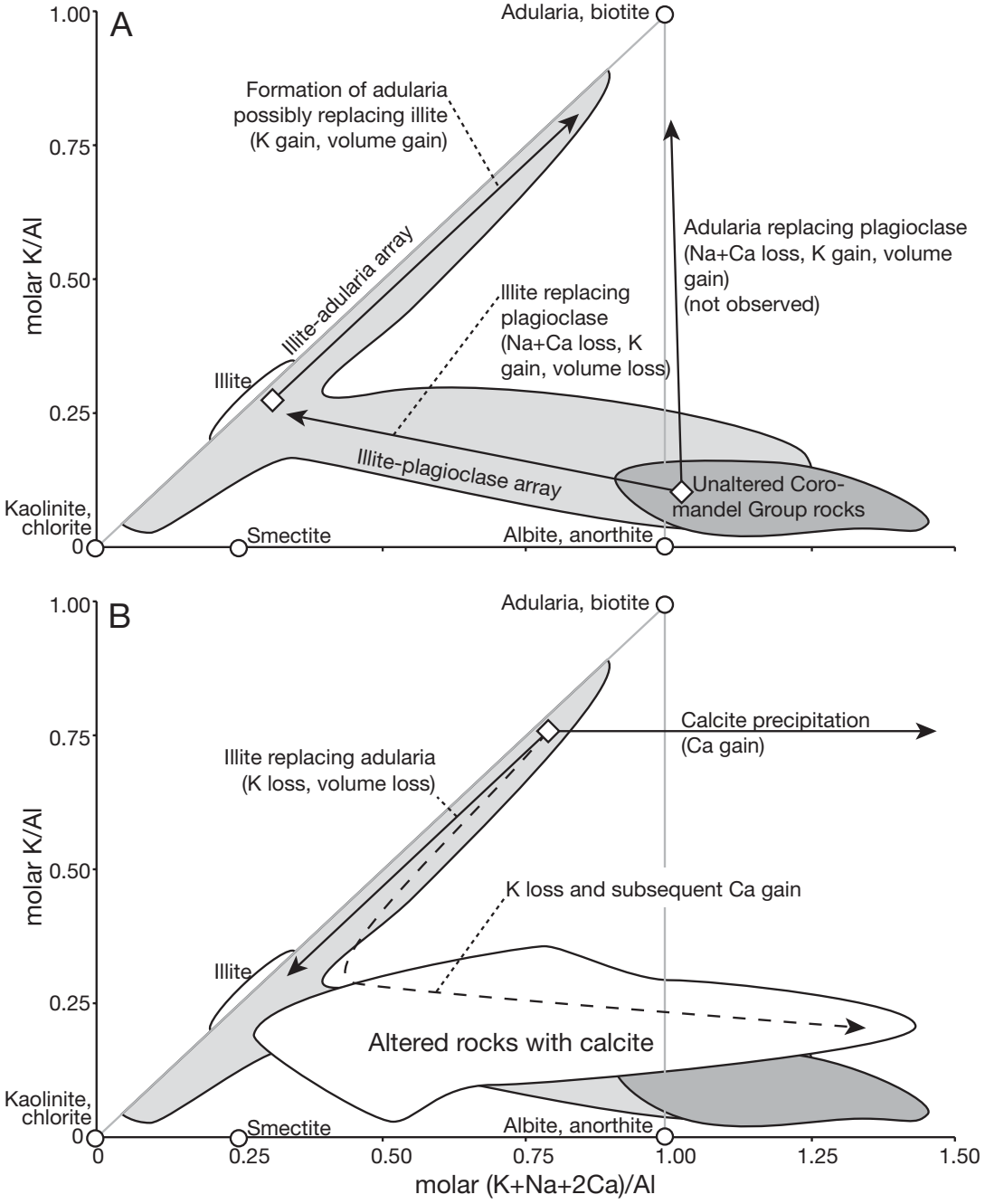

FIG. 11. Bivariate diagrams of *M* (K + Na + 2Ca)/Al against *M* K/Al. Circles indicate ideal mineral compositions. A. Schematic of main-stage hydrothermal alteration. Fields represent unaltered Coromandel Group rocks and altered rocks of the Waitekauri prospect excluding those with calcite. B. Schematic of late-stage alteration. White field represents all altered rocks that contain calcite.

run to completion in every adularia-rich rock that we studied in the area (Fig. 11A). Although this seems unlikely, we offer this interpretation, in addition to the interpretation that adularia only forms in illite-dominated rocks, because it is more consistent with petrographic data. Our geochemical data could support either option.

Volume change associated with alteration

The volume change of hydrothermal reactions can be calculated based on the reaction coefficients and molar volumes of the solid phases, given that the liquid and dissolved phases are lost in an open system (Stanley et al., in press). We use molar volume data of Holland and Powell (1998) for minerals under metamorphic conditions. The minerals have approximately the same relative molar volumes regardless of P, so the same data can be applied to minerals in a shallow epithermal deposit (Berman, 1988). We identify sets of alteration reactions for the illite-plagioclase and the illite-adularia arrays. These sets are not exhaustive but summarize the hydrothermal alteration processes along the arrays, on the assumption that Al is conserved, for a plagioclase + clinopyroxene andesitic source rock. For the illite-plagioclase array:

$$\underset{\text{Albite}}{3NaAlSi_3O_8} + 2H^+_{(aq)} + K^+_{(aq)} \leftrightarrows \underset{\text{Illite}}{KAl_3Si_3O_{10}(OH)_2} + 3Na^+_{(aq)} + \underset{\text{Quartz}}{6SiO_2}, \quad (2)$$

$$\underset{\text{Anorthite}}{3CaAl_2Si_2O_8} + 4H^+_{(aq)} + 2K^+_{(aq)} \leftrightarrows \underset{\text{Illite}}{2KAl_3Si_3O_{10}(OH)_2} + 3Ca^+_{(aq)}, \quad (3)$$

$$\underset{\text{Clinopyroxene}}{5CaMgSi_2O_6} + 2NaAlSi_3O_8 + 10H^+ \leftrightarrows \underset{\text{Albite}}{Mg_5Al_2Si_3O_{10}(OH)_8} + 5Ca^{2+}_{(aq)} + 2Na^+_{(aq)} + \underset{\text{Quartz}}{13SiO_2} + 2H_2O, \quad (4)$$

$$\underset{\text{Clinopyroxene}}{5CaMgSi_2O_6} + \underset{\text{Anorthite}}{CaAl_2Si_2O_8} + 12H^+ \leftrightarrows \underset{\text{Chlorite}}{Mg_5Al_2Si_3O_{10}(OH)_8} + 6Ca^{2+}_{(aq)} + \underset{\text{Quartz}}{9SiO_2} + 2H_2O. \quad (5)$$

The alteration of anorthite and albite to illite and quartz (eq. 2 and 3) constitute volume decreases of ca. –8 percent. The alteration of diopsidic clinopyroxene and plagioclase to chlorite and quartz also results in volume decreases of –8 percent (eq. 4) and –4 percent (eq. 5). Progressive alteration of rocks along the illite-plagioclase array therefore leads to a net volume decrease of the altered rock body. Despite the volume decrease, the density of the rocks also decreases because massive, intermediate igneous rock (density >2.7 g/cm^3) is altered to rock with a density in the range 2.2 to 2.7 g/cm^3 (at the Golden Cross epithermal deposit; Simpson and Mauk, 2000). Volume and density can both decrease during the alteration process because on average the altered rocks lose soluble elements to the hydrothermal fluid resulting in a net mass loss, as noted above.

For the illite-plagioclase array, the principal reaction is the replacement of illite by adularia or vice versa:

$$\underset{\text{K mica}}{KAl_3Si_3O_{10}(OH)_2} + 2K^+_{(aq)} + \underset{\text{Quartz}}{6SiO_2} \leftrightarrows \underset{\text{Adularia}}{3KAlSi_3O_8} + 2H^+_{(aq)}. \quad (6)$$

The alteration of illite to adularia and quartz leads to a 15 percent vol increase; the reverse reaction, replacement of adularia by illite, which is commonly observed (Simpson and Mauk, 2011), leads to a concomitant volume decrease. Late-stage calcite precipitation may be facilitated by that volume decrease, consistent with the observation that calcite does not occur in adularia-rich (high K/Al) rocks (Fig. 11B).

The negative volume change that accompanies illite-chlorite replacement of an igneous plagioclase-pyroxene assemblage can help to explain why illite altered rocks in the Waitekauri area extend to kilometers away from the central upwelling zone along the Waitekauri fault. The reactions in equations (2) to (5) create space, through which a hydrothermal fluid can permeate. This in turn promotes further hydrothermal alteration of the rock body and allows the alteration zone to expand outward from a central upwelling zone. In contrast, replacement of illite by adularia as the dominant K-bearing alteration mineral has an associated volume increase and makes the rock body less permeable as fluid pathways become sealed. This inhibits further hydrothermal fluid interaction. Widespread adularia alteration can therefore only occur when fluid pathways are continually opened by tectonic activity to offset the self-sealing character of the reaction. In the Waitekauri area, abundant adularia precipitated mostly at Sovereign around the central Waitekauri fault. The more outlying alteration cell at Scotia developed a smaller adularia-rich rock volume, and rocks there experienced lesser K gains. As a result, maximum and average K_2O and SiO_2 mass gains and K/Sr, Rb/Sr, and *M* K/(K + Na + 2Ca) values in altered rocks vector from the periphery of the Waitekauri area toward the center of the alteration zone.

Size of the data set and application to other districts

This paper is based on an extensive data set of samples from numerous drill holes along a 3-km-wide section. Typical exploration data sets may be less exhaustive and the obtained geochemical vectors less conclusive. Nevertheless, the present approach to mass-change calculation can be valuable in smaller data sets, if its principal use is the identification the maximum mass change experienced by rocks in a particular altered area. An exploration geologist can distinguish areas where significant alteration to adularia occurred and within each such area, rocks with adularia and without calcite are the most likely to have preserved large K enrichments from the peak phase of hydrothermal alteration. Selective obtainment and analysis of such rocks can provide a data set that documents the maximum magnitude of K enrichment. Comparison of the maximum K enrichments across an alteration zone can then determine whether a regional trend exists. In such a selective data set, both the average and maximum K gain values would show the same trend. In the Waitekauri area data set, the trend in average K gain values reflects the trend in maximum K gain values but is less pronounced because we analyzed a spectrum of rocks instead of only the most strongly K metasomatized rocks.

The regression equations presented in Table 3 are based on a cross section of the Coromandel Group volcanic succession. They are consequently applicable to all typical Coromandel Group rocks, which are the most likely host for new discoveries in the Hauraki goldfield. Application in other districts

where medium potassic, calc-alkaline andesites and dacites host mineralization is possible as a way of obtaining an estimate of mass changes. However, at given SiO_2 concentration, K_2O concentrations vary considerably between suites of arc volcanic rocks (Gill, 1981). Calibration to local unaltered or least altered baseline rock compositions therefore remains a necessary precondition for a precise estimate of K_2O gains. Nonetheless, several other parameters, including K/Sr, Rb/Sr, and M K/(K + Na + 2Ca) values can quantify relative K gains.

Conclusions

We used an extensive geochemical data set to map the compositions of unaltered rocks throughout the volcanic stratigraphy of andesites and dacites in the Hauraki goldfield. These rocks show a consistent relationship between major element composition and values of the immobile element ratio Zr/TiO_2, and we used this feature to back-calculate the initial composition of equivalent, veinless altered rocks in the Waitekauri area. The total transferred mass is equal to ca. 11 percent of rock mass in illite-dominated rocks, whereas in intensely metasomatized adularia-bearing rocks it is ca. 24 percent of rock mass. On average, altered rocks throughout the Waitekauri area lost mass. Maximum and average K_2O, SiO_2, and Rb gains are insignificant or low in weakly to moderately altered rocks at outlying prospect areas and reach maxima in adularia-rich rocks that surround Au deposits along the Waitekauri fault, showing that K metasomatism increases across a 3-km-wide section from the periphery to the center of the Waitekauri area. Average and maximum K/Sr, Rb/Sr, and M K/(K + Na + 2Ca), and K/Al values correlate with K_2O and SiO_2 mass gain, and together these parameters vector toward adularia-rich rocks that host epithermal Au deposits at the center of the Waitekauri altered area.

Acknowledgments

We thank Heritage Gold New Zealand, Ltd., Newmont Waihi Operations, and the New Zealand Foundation for Research, Science and Technology for supporting this research. Unaltered Coromandel Group rock samples were in part provided by R.M. Briggs of the University of Waikato and R.L. Brathwaite, A.B. Christie, and D.N.B. Skinner of GNS Science, Ltd. Newmont Waihi Operations provided access to Waitekauri area drill core. Reviews by I. Warren, N.J. Olsen, and D. John, and editorial control by L. Meinert greatly improved an earlier version of this manuscript.

REFERENCES

Adams, C.J., Graham, I.J., Seward, D., and Skinner, D.N.B., 1994, Geochronological and geochemical evolution of late Cenozoic volcanism in the Coromandel peninsula, New Zealand: New Zealand Journal of Geology and Geophysics, v. 37, p. 359–378.

Baalen, M.R., 1993, Titanium mobility in metamorphic systems: A review: Chemical Geology, v. 110, p. 233–249.

Berman, R.G., 1988, Internally consistent thermodynamic data for minerals in the system: Na_2O-K_2O-CaO-MgO-FeO-Fe_2O_3-Al_2O_3-SiO_2-TiO_2-H_2O-CO_2: Journal of Petrology, v. 29, p. 455–522.

Brathwaite, R.L., and Christie, A.B., 1996, Geology of the Waihi area, sheet T13BD and part U13, scale 1:50 000: Institute of Geological and Nuclear Sciences, Ltd.

Brenan, J.M., Shaw, H.F., Ryerson, F.J., and Phinney, D.L., 1995, Experimental determination of trace element partitioning between pargasite and a synthetic andesitic melt: Earth and Planetary Science Letters, v. 135, p. 1–11.

Briggs, R.M., Houghton, B.F., McWilliams, M., and Wilson, C.J.N., 2005, $^{40}Ar/^{39}Ar$ ages of silicic volcanic rocks in the Tauranga-Kaimai area, New Zealand: Dating the transition between volcanism in the Coromandel arc and the Taupo volcanic zone: New Zealand Journal of Geology and Geophysics, v. 48, p. 459–469.

Carlile, J.C., Davey, G.R., Kadir, I., Langmead, R.P., and Rafferty, W.J., 1998, Discovery and exploration of the Gosowong epithermal gold deposit, Halmahera, Indonesia: Journal of Geochemical Exploration, v. 60, p. 207–227.

Carmichael, I.S.E., 2002, The andesite aqueduct: perspectives on the evolution of intermediate magmatism in west-central (105-99° W) Mexico: Contributions to Mineralogy and Petrology, v. 143, p. 641–663.

Cartledge, G.H., 1928, Studies on the periodic system, I. The ionic potential as a periodic function: Journal of the American Chemical Society, v. 50, p. 2856–2872.

Chambefort, I., Moritz, R., and von Quadt, A., 2007, Petrology, geochemistry and U-Pb geochronology of magmatic rocks from the high-sulfidation epithermal Au-Cu Chelopech deposit, Srenogorie zone, Bulgaria: Mineralium Deposita, v. 42, p. 665–690.

Charlier, B.L.A., Wilson, C.J.N., Lowenstern, J.B., Blake, S., van Calsteren, P.W., and Davidson, J.P., 2005, Magma generation at a large, hyperactive silicic volcano (Taupo, New Zealand) revealed by U-Th and U-Pb systematics in zircons: Journal of Petrology, v. 46, p. 3–32.

Christie, A.B., Simpson, M.P., Brathwaite, R.L., Mauk, J.L., and Simmons, S.F., 2007, Epithermal Au-Ag and related deposits of the Hauraki goldfield, Coromandel volcanic zone, New Zealand: Economic Geology, v. 102, p. 785–816.

Clarke, D.S., and Govett, G.J.S., 1990, Southwest Pacific epithermal gold: A rock geochemistry prospective: Journal of Geochemical Exploration, v. 35, p. 225–240.

Cox, S.F., Knackstedt, M.A., and Braun, J., 2001, Principles of structural control on permeability and fluid flow in hydrothermal systems: Reviews in Economic Geology, v. 14, p. 1–24.

Davidson, J.P., Turner, S., Handley, H., Macpherson, C., and Dosseto, A., 2007, Amphibole "sponge" in arc crust?: Geology, v. 35, p. 787–790.

Downey, J.F., 1935, Gold mines of the Hauraki district: Wellington, New Zealand, Government Printer, 315 p.

Edbrooke, S.W., 2001, Geology of the Auckland area: Institute of Geological and Nuclear Sciences, Geological Map, 3, scale 1:250,000.

Ewart, A., and Griffin, W.L., 1994, Application of proton-microprobe data to trace element partitioning in volcanic rocks: Chemical Geology, v. 117, p. 251–284.

Finlow-Bates, T., and Stumpfl, E.F., 1981, The behavior of so-called immobile elements in hydrothermally altered rocks associated with volcanogenic submarine-exhalative deposits: Mineralium Deposita, v. 16, p. 319–328.

Gemmell, J.B., 2007, Hydrothermal alteration associated with the Gosowong epithermal Au-Ag deposit, Halmahera, Indonesia: Mineralogy, geochemistry and exploration implications: Economic Geology, v. 102, p. 893–922.

Giggenbach, W.F., 1984, Mass transfer in hydrothermal alteration systems—a conceptual approach: Geochimica et Cosmochimica Acta, v. 45, p. 393–410.

Giggenbach, W.F., 1988, Geothermal solute equilibria: Derivation of Na-K-Mg-Ca geoindicators: Geochimica et Cosmochimica Acta, v. 52, p. 2749–2765.

Gill, J.B., 1981, Orogenic andesites and plate tectonics: Berlin-Heidelberg, Springer-Verlag.

Gresens, R.L., 1967, Composition-volume relationships of metasomatism: Chemical Geology, v. 2, p. 47–65.

Hallberg, J.A., 1984, A geochemical aid to igneous rock type identification in deeply-weathered terrain: Journal of Geochemical Exploration, v. 20, p. 1–8.

Haworth, A.V., and Briggs, R.M., 2006, Epithermal Au-Ag mineralisation in the Lower Waitekauri Valley, Hauraki goldfield: Australasian Institute of Mining and Metallurgy Monograph 25, p. 157–162.

Hedenquist, J.W., Arribas, A., and Gonzales-Urien, E., 2000, Exploration for epithermal gold deposits: Reviews in Economic Geology, v. 13, p. 245–277.

Hickmott, D., and Spear, F.S., 1992, Major and trace element zoning in garnets from calcareous pelites in the NW Shelbourne Falls quadrangle, Massachussetts: Garnet growth histories in retrograde rocks: Journal of Petrology, v. 33, p. 965–1005.

Holland, T.J.B., and Powell, R., 1998, An internally consistent thermodynamic data set for phases of petrological interest: Journal of Metamorphic Geology, v. 16, p. 309–343.

Jiang, S., Wang, R., Xu, X., and Zhao, K., 2005, Mobility of high-field strength elements (HFSE) in magmatic- metamorphic-, and submarine-hydrothermal systems: Physics and chemistry of the Earth, v. 30, p. 1020–1029.

John, D.A., Hofstra, A.H., Fleck, R.J., Brummer, J.E., and Saderholm, E.C., 2003, Geologic setting and genesis of the Mule Canyon low-sulfidation epithermal gold-silver deposit, north-central Nevada: Economic Geology, v. 98, p. 425–463.

Johnson, K.T.M., and Kinzler, R.J., 1989, Partitioning of REE, Ti, Zr, Hf, and Nb between clinopyroxene and basaltic liquid: An ion microprobe study: EOS, v. 70, p. 1388.

Le Bas, M.J., Le Maitre, R.W., Streckeisen, A., and Zanettin, B., 1986, A chemical classification of volcanic rocks based on the total alkali silica diagram: Journal of Petrology, v. 27, p. 745–750.

Leavitt, E.D., and Arehart, G.B., 2005, Alteration, geochemistry and paragenesis of the Midas epithermal gold-silver deposit, Elko County, Nevada: Geological Society of Nevada Symposium, Reno, Nevada, May 2005, Proceedings, p. 563–627.

MacLean, W.H., 1990, Mass changes calculations in altered rock series: Mineralium Deposita, v. 25, p. 44–49.

Madeisky, H.E., 1996, A lithogeochemical and radiometric study of hydrothermal alteration and metal zoning at the Cinola epithermal gold deposit, Queen Charlotte Islands, British Columbia, *in* Coyner, A.R., and Fahey, P.L., eds., Geology and ore deposits of the American Cordillera, v. 3, p. 1153–1185.

Mauk, J.L., and Simpson, M.P., 2007, Geochemistry and stable isotope composition of altered rocks at the Golden Cross epithermal Au-Ag deposit, New Zealand: Economic Geology, v. 102, p. 841–871.

Mauk, J.L., Hall, C.M., Chesley, J.T., and Barra, F., 2011, Punctuated evolution of a large epithermal province: The Hauraki goldfield, New Zealand: Economic Geology, v. 106, p. 921–943.

Morrell, A.E., Locke, C.A., Cassidy, J., and Mauk, J.L., 2011, Geophysical characteristics of adularia-sericite epithermal gold-silver deposits in the Waihi-Waitekauri region, New Zealand: Economic Geology, v. 106, p. 1031–1041.

Murphy, D.M.K., and Stanley, C.R., 2007, Lithogeochemical constraints on the host rock, hydrothermal alteration and weathering of the Groundrush gold deposit: Geochemistry: Exploration, Environment, Analysis, v. 7, p. 363–375.

Okamoto, K., 1979, Geochemical study on magmatic differentiation of Asama volcano, central Japan: Journal of the Geological Society of Japan, v. 85, p. 525–535.

Person, M., Banerjee, A., Hofstra, A., Sweetkind, D., and Gao, Y., 2008, Hydrologic models of modern and fossil geothermal systems in the Great Basin: Genetic implications for epithermal Au-Ag and Carlin-type gold deposits: Geosphere, v. 4, p. 888–917.

Price, R.C., Gamble, J.A., Smith, I.E.M., Stewart, R.B., Eggins, S., and Wright, I.C., 2005, An integrated model for the temporal evolution of andesites and rhyolites and crustal development in New Zealand's North Island: Journal of Volcanology and Geothermal Research, v. 140, p. 1–24.

Rosenberg, M.D., Bignall, G., and Rae, A.J., 2009, The geologic framework of the Wairakei-Tauhara geothermal system, New Zealand: Geothermics, v. 38, p. 72–84.

Sherlock, R.L., 1996, Hydrothermal alteration of volcanic rocks at the McLaughlin gold deposit, northern California: Canadian Journal of Earth Sciences, v. 33, p. 493–508.

Shikazono, N., Yonekawa, N., and Karakizawa, T., 2002, Mass transfer, oxygen isotopic variation and gold precipitation in an epithermal system: A case study of the Hishikari deposit, southern Kyushu, Japan: Resource Geology, v. 52, p. 21 1–222.

Shimizu, N., and Kushiro, I., 1975, Partitioning of rare-earth elements between garnet and liquid at high pressures—preliminary experiments: Geophysical Research Letters, v. 2, p. 413–416.

Simmons, S.F., and Browne, P.R.L., 2000, Hydrothermal minerals and precious metals in the Broadlands-Ohaaki geothermal system: Implications for understanding low-sulfidation epithermal environments: Economic Geology, v. 95, p. 971–999.

Simpson, M.P., and Mauk, J.L., 2000, Geochemistry of wall rock alteration at the Golden Cross deposit, New Zealand: New Zealand Minerals and Mining Conference, Wellington, New Zealand, Proceedings, p. 197–208.

——2011, Hydrothermal alteration and veins at the epithermal Au-Ag deposits and prospects of the Waitekauri area, Hauraki goldfield, New Zealand: Economic Geology, v. 106, p. 945–973.

Sisson, T.W., 1991, Pyroxene-high silica rhyolite trace element partition coefficients measured by ion microprobe: Geochimica et Cosmochimica Acta, v. 55, p. 1575–1585.

——1994, Hornblende-melt trace element partitioning measured by ion microprobe: Chemical Geology, v. 117, p. 33 1–344.

Skinner, D.N.B., 1986, Neogene volcanism of the Hauraki volcanic region: Royal Society of New Zealand Bulletin, v. 23, p. 21–47.

Spörli, K.B., Begbie, M.J., Irwin, M.R., and Rowland, J.V., 2006, Structural processes and tectonic controls on the epithermal Au-Ag deposits of the Hauraki goldfield: Australasian Institute of Mining and Metallurgy Monograph 25, p. 85–94.

Stanley, C.R., Baker, T., Mustard, R., Radford, N., and Butler, I., in press, Lithogeochemistry of hydrothermally altered host rocks at the Pajingo low sulfidation gold deposit, Queensland, Australia: The geochemical anatomy of an epithermal alteration zone: Gechemistry: Exploration, Environment, Analysis.

Stipp, J.J., 1968, The geochronology and petrogenesis of the Cenozoic volcanics of North Island, New Zealand: Unpublished Ph.D. thesis, Australian National University.

Sun, S.S., and McDonough, W.F., 1989, Chemical and isotopic systematics of oceanic basalts: Implications for mantle composition and processes: Geological Society of London Special Publication, v. 42, p. 313–345.

Warren, I., Simmons, S.F., and Mauk, J.L., 2007, Whole-rock geochemical techniques for evaluating hydrothermal alteration, mass changes, and compositional gradients associated with epithermal Au-Ag mineralization: Economic Geology, v. 102, p. 923–948.

Watson, E.B., and Harrison, T.M., 1983, Zircon saturation revisited: Temperature and composition effects in a variety of crustal magma types: Earth and Planetary Science Letters, v. 64, p. 295–304.

White, N.C., and Hedenquist, J.W., 1995, Epithermal gold deposits: styles, characteristics and exploration: Society of Economic Geology Newsletter 23, p. 1–13.